

The Weak Patch Test for Nonhomogeneous Materials Modeled with Graded Finite Elements

Glaucio H. Paulino

paulino@uiuc.edu
University of Illinois at Urbana
Champaign
Dept. of Civil and Environmental Eng.
Urbana, IL 61801. USA

Jeong-Ho Kim

jhkim@enr.uconn.edu
University of Connecticut
Dept. of Civil and Environmental Eng.
Storrs, CT 06269. USA

Functionally graded materials have an additional length scale associated to the spatial variation of the material property field which competes with the usual geometrical length scale of the boundary value problem. By considering the length scale of nonhomogeneity, this paper presents the weak patch test (rather than the standard one) of the graded element for nonhomogeneous materials to assess convergence of the finite element method (FEM). Both consistency (as the size of elements approach zero, the FEM approximation represents the exact solution) and stability (spurious mechanisms are avoided) conditions are addressed. The specific graded elements considered here are isoparametric quadrilaterals (e.g. 4, 8 and 9-node) considering two dimensional plane and axisymmetric problems. The finite element approximate solutions are compared with exact solutions for nonhomogeneous materials.

Keywords: finite element method (FEM), patch test, weak patch test, functionally graded material (FGM), graded element

Introduction

The *patch test* was originated by the memorable Bruce Irons and coworkers (Irons, 1966; Bazeley *et al.*, 1966; Irons and Razzaque, 1972). The concept is so important that it can be easily found in many textbooks in finite elements, either classical (Hughes, 1987; Cook *et al.*, 2002; Bathe, 1995) or more recent (Belytschko *et al.*, 2000; Zienkiewicz and Taylor, 2000) ones, and it is needed to ensure reliability of the finite element method (FEM) (Babuška and Strouboulis, 2001). The original patch test provided a necessary consistency condition and thus turned out to be very useful for assessing convergence of finite elements analysis, including nonconforming elements (Wilson *et al.*, 1973; Taylor *et al.*, 1976; Taylor *et al.*, 1986). An early mathematical treatment was given by Strang (1972), and Strang and Fix (1973). For an element which appears to be convergent but fails the Iron's patch test, the weak patch test is an alternative test, as suggested by Taylor *et al.* (1986). In addition, Belytschko and Lasry (1988) have studied the behavior of a distorted element with a fractal patch test, which is also valid in the weak patch test sense. The patch test has been applied to many problem-types including, for example, mixed displacement-pressure finite element formulations (Taylor *et al.*, 1986; Zienkiewicz *et al.*, 1986; Razzaque, 1986; Wu and Chen, 1997; Zienkiewicz and Taylor, 1997), three-dimensional (3-D) solid elements (Loikkanen and Irons, 1984), plate bending elements (Samuelsson *et al.*, 1987; Zienkiewicz and Lefebvre, 1988; Zhifei, 1993; Zienkiewicz *et al.*, 1993; Auricchio and Taylor, 1993; Auricchio and Taylor, 1994; Martins and Sabino, 1997; Park and Choi, 1997), and shell elements (Herrmann, 1989). The patch test has also been used as a fundamental tool to create new elements or to improve existing ones (Ju and Sin, 1996; Cheung *et al.*, 2002; Piltner and Taylor, 2000).

The patch test has become a widely used procedure, which can be numerically performed, in order to check the validity of a finite element formulation and coding. It is the necessary and sufficient condition for finite element analysis convergence (Zienkiewicz and Taylor, 2000). For sufficiency, at least one internal element boundary is required to verify that consistency of a patch solution is maintained between elements. To ensure convergence, both consistency and stability conditions must be verified. The consistency requirement ensures that as the size of the elements h tends to zero, the finite element approximation represents the exact

solution. The stability condition is a requirement that an element admits no zero-energy mode deformation states when adequately supported against rigid-body motion, which means that the element stiffness matrix ($\mathbf{\kappa}^e$) must be non-singular. Stability is usually checked by ensuring that the stiffness matrix is of appropriate rank, and thus doesn't allow for appearance of spurious mechanisms.

Modeling of functionally graded materials (FGMs) by the FEM can be accomplished by using either graded or homogeneous elements (Santare and Lambros, 2000; Kim and Paulino 2002a), as illustrated by Fig. 1. Part (a) of this figure shows an example of an exponentially graded material and part (b) illustrates an L-shaped domain made of this material. The graded element (see Fig. 1(c)) incorporates the material property gradient at the size scale of the element, while the homogeneous element (see Fig. 1(d)) produces a step-wise constant approximation to a continuous material property field. The patch test has been used to verify convergence of conventional homogeneous elements (Fig. 1(d)). In order to assess convergence of the graded elements, they must be patch-tested in the context of the "weak patch test".

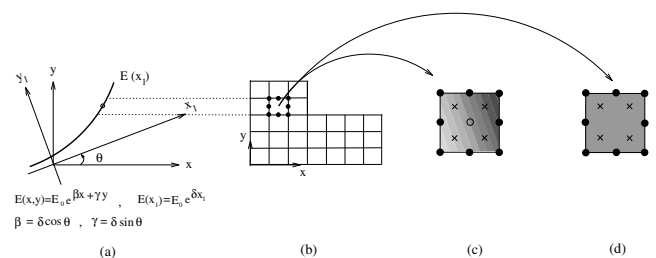


Figure 1. FEM modeling of FGMs: (a) nonhomogeneous medium; (b) generic region, e.g. L-shaped domain; (c) graded element; (d) homogeneous element. The property of the homogeneous elements may be taken as the actual property at the centroid of the element (cf. (c) and (d)). Here the symbol • means a nodal point, and the symbol × means a Gauss sampling point. The symbol o indicates the location for material property sampling (see parts (a) and (c)).

Various finite element investigations of graded materials have been conducted using either commercially available (e.g. ABAQUS, ANSYS) or research-oriented codes. A sampling (which is, by no means, exhaustive) of published papers include a broad range of applications such as elasticity (Santare and Lambros, 2000; Kim and Paulino 2002a); linear elastic fracture mechanics (Eischen, 1987; Gu *et al.*, 1999; Anlas *et al.*, 2000; Kim and Paulino, 2002b, 2003, 2004, 2005; Paulino and Kim, 2004); nonlinear fracture mechanics

(Carpenter *et al.*, 1999; Kim *et al.*, 1997); cohesive zone elements for fracture of FGMs (Jin *et al.*, 2002; Zhang and Paulino, 2005); notch effect on FGM specimens (Lin and Miyamoto, 2000); tribology (Stephens *et al.*, 2000; Jitcharoen *et al.*, 1998); thermal stresses (Giannakopoulos *et al.*, 1995; Cho and Oden, 2000; Cho and Ha, 2001; Noda, 1999); residual stresses (Lee and Erdogan, 1995; Williamson *et al.*, 1993; Becker *et al.*, 2000; Khor and Gu, 2000); various aspects of micromechanical modeling (Grujicic and Zhang, 1998; Dao *et al.*, 1997; Shen, 1998); numerical homogenization (Schmauder and Weber, 2001; LeBlé *et al.*, 1999); sensitivity analysis and optimization (Tanaka *et al.*, 1996); evaluation of the so called “higher order theory” (Pindera and Dunn, 1997); and functionally graded piezoelectric actuators (Almajid *et al.*, 2001; Carbonari *et al.*, 2006a, 2006b).

In particular, the use of graded finite elements is of direct relevance to this work. Such elements were used by Santare and Lambros (2000) to model the behavior of nonhomogeneous elastic materials, and by Lee and Erdogan (1995) to investigate residual/thermal stresses in FGMs and thermal barrier coatings. Both authors (Santare and Lambros, 2000; Lee and Erdogan, 1995) used the Gauss point sampling of material properties. Graded elements were also used by Kim and Paulino (2003, 2004, 2005) and Paulino and Kim (2004) to investigate fracture mechanics of FGMs and to model nonhomogeneous isotropic and orthotropic materials, however, they have employed a generalized isoparametric formulation (Kim and Paulino, 2002a).

The goal of the remainder of this paper is to develop a comprehensive presentation of the weak patch test for nonhomogeneous materials modeled with graded finite elements, and assess convergence rate of graded elements. This paper is organized as follows. First, we provide some exact solutions for nonhomogeneous elasticity that will be used as reference solutions for numerical examples. Then we present the graded element formulations, and various examples on the weak patch test, and also assess convergence rate. Finally we address stability considerations for graded finite elements followed by conclusions of the present investigation.

Exact Solutions for Nonhomogeneous Elasticity: Reference Solutions

This section revisits a few closed-form solutions for nonhomogeneous elasticity problems. Two classes of problems are considered: plane and axisymmetric. In the first class, we consider an infinitely long plate, graded along its finite width, under symmetric loading conditions (fixed grip, tension, and bending) and also a simple shear problem. In the second class, we consider an axisymmetric problem, graded along the radial direction, under axisymmetric loading conditions. These closed-form solutions will be used as reference solutions for the weak patch test.

Plane Problems

Erdogan and Wu (1997) derived exact solutions for stresses to plane elasticity problems involving functionally graded plates of infinite length and finite width under symmetric loading conditions such as fixed grip, tension, and bending away from the center region of the specimen (see Fig. 2). Kim and Paulino (2002a) extended the work to orthotropic FGMs, and provided exact solutions for displacements. Let's consider the graded plate illustrated by Fig. 2, and let's assume the Poisson's ratio as constant. The shear modulus is given by

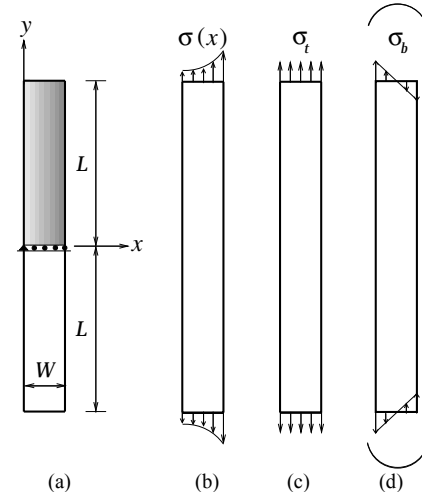


Figure 2. A graded strip: (a) geometry – the shaded region indicates the symmetric region of the plate used in the present FEM analyses ($u_x(a,0) = u_x(a,L) = 0$ with $a = 0$ where “a” denotes the x coordinate.); (b) fixed-grip loading; (c) tension; (d) bending.

$$\mu(x) = \mu_1 e^{\beta x}, \quad \mu_1 = \frac{E_1}{2(1+\nu)}, \tag{1}$$

where $1/\beta$ is the length scale of the nonhomogeneity, which is characterized by

$$\beta = \frac{1}{W} \log\left(\frac{E_2}{E_1}\right) \tag{2}$$

with $E=E(x)$ where $E_1 = E(x=0)$ and $E_2 = E(x=W)$.

Fixed Grip Loading

For fixed grip loading (Fig. 2(b)) with $\varepsilon_{yy}(x, \pm\infty) = \varepsilon_0$, the stress is given by

$$\sigma_{yy}(x) = \frac{8\mu(x)}{1+\kappa} \varepsilon_0, \tag{3}$$

where $\kappa = 3 - 4\nu$: plane strain
 $\kappa = (3 - \nu)/(1 + \nu)$: plane stress.

Using the strain-displacement relations and applying the following boundary conditions

$$u_x(a,0) = 0, \quad u_y(x,0) = 0, \tag{4}$$

where the parameter a denotes a reference point for the displacement boundary condition, one obtains the following displacement fields

$$u_x(x,y) = \frac{\kappa - 3}{1 + \kappa} \varepsilon_0 (-x + a) \tag{5}$$

$$u_y(x,y) = \varepsilon_0 y.$$

Notice that the displacement fields are linear and thus strains are constant; however, stresses vary exponentially.

Tension and Bending

For tension (Fig. 2(c)) and bending (Fig. 2(d)) loads applied perpendicular to material gradation, the applied stresses are defined by

$$N = \sigma_t W, \quad M = \frac{\sigma_b W^2}{6}, \tag{5}$$

where N is a membrane resultant applied along the $x = W/2$ line, and M is the bending moment. An infinitely long strip under these two loading cases can be considered as one-dimensional problem where $\sigma_{xx} = \sigma_{xy} = 0$, and $\sigma_{yy} \neq 0$. Thus the compatibility condition $\partial^2 \varepsilon_{yy} / \partial x^2 = 0$ gives

$$\sigma_{yy}(x) = \frac{8\mu(x)}{1+\kappa}(Ax+B), \tag{7}$$

where the constants A and B are determined from

$$\int_0^W \sigma_{yy}(x) dx = N, \quad \int_0^W \sigma_{yy}(x) x dx = M \tag{8}$$

by assuming

$$M = NW/2 \text{ for tension and } N = 0 \text{ for bending.} \tag{9}$$

Thus, for *tension* load, the constants A and B are:

$$A = \frac{\beta N (1+\kappa)}{16\mu_1} \left(\frac{W\beta^2 e^{\beta W} - 2\beta e^{\beta W} + W\beta^2 + 2\beta}{e^{\beta W} \beta^2 W^2 - e^{2\beta W} + 2e^{\beta W} - 1} \right), \tag{10}$$

$$B = \frac{\beta N (1+\kappa)}{16\mu_1} \left(\frac{-W^2 \beta^2 e^{\beta W} + 3W\beta e^{\beta W} - 4W e^{\beta W} + W\beta + 4}{e^{\beta W} \beta^2 W^2 - e^{2\beta W} + 2e^{\beta W} - 1} \right),$$

respectively. For *bending* load, the constants A and B are:

$$A = \frac{\beta^2 M (1+\kappa)}{8\mu_1} \left(\frac{\beta(1-e^{\beta W})}{e^{\beta W} \beta^2 W^2 - e^{2\beta W} + 2e^{\beta W} - 1} \right), \tag{11}$$

$$B = \frac{\beta^2 M (1+\kappa)}{8\mu_1} \left(\frac{\beta W e^{\beta W} - e^{\beta W} + 1}{e^{\beta W} \beta^2 W^2 - e^{2\beta W} + 2e^{\beta W} - 1} \right),$$

respectively.

Using the strain-displacement relations and applying the boundary conditions given by Eq.(4), one obtains the following displacement field

$$u_x(x,y) = \frac{\kappa-3}{1+\kappa} \left(\frac{A}{2} x^2 + Bx - \frac{A}{2} a^2 - Ba \right) - \frac{A}{2} y^2, \tag{12}$$

$$u_y(x,y) = (Ax+B)y.$$

Simple Shear

Figure 3 shows a graded plate under uniform simple shear load, i.e. $\sigma_{xy} = \tau = 1.0$. Assume that the Poisson's ratio is constant, and the shear modulus varies in the y direction as follows:

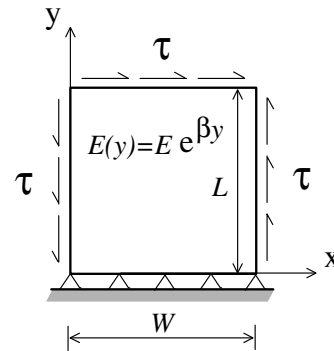


Figure 3. A functionally graded plate under constant shear ($\sigma_{xy} = \tau = 1.0$).

$$\mu(y) = \mu_1 e^{\beta y}. \tag{13}$$

Because $\sigma_{yy} = 1.0$ everywhere, the shear strain distribution becomes

$$\varepsilon_{xy} = \frac{1}{2\mu(y)} = \frac{1}{2\mu_1} e^{-\beta y}. \tag{14}$$

Using the strain-displacement relations and applying the boundary conditions:

$$u_x(x,0) = u_y(x,0) = 0,$$

one obtains the following displacement field

$$u_x(x,y) = \frac{1}{\mu_1 \beta} (1 - e^{-\beta y}), \quad u_y(x,y) = 0. \tag{15}$$

Axisymmetric Problem

Horgan and Chan (1999) provided exact solutions for stresses for a hollow circular cylinder subjected to uniform pressure p_i and p_o on the inner ($r_i = a$) or outer ($r_o = b$) surfaces, respectively (see Fig. 4). They assumed power-law variation of Young's modulus given by

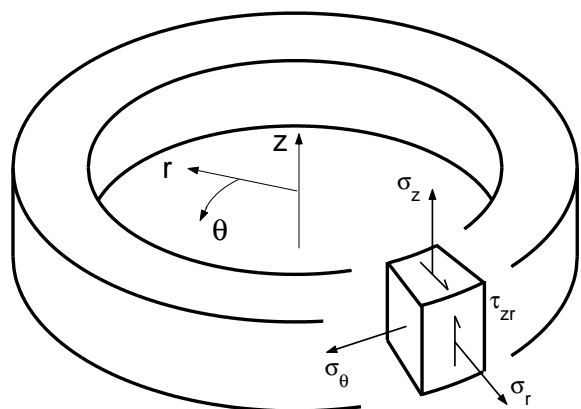


Figure 4. An axially symmetric hollow cylinder or disk.

$$E(r) = E_1 \left(\frac{r}{a} \right)^n \tag{16}$$

with $E_1 = E(a)$ and the power n being a dimensionless constant. The displacements are given by:

$$u(r) = C_1 r^{-(n+k)/2} + C_2 r^{-(n-k)/2}, \quad k = (n^2 + 4 - 4nv)^{1/2}, \tag{17}$$

where C_1 and C_2 are constants which can be determined by applying the axisymmetric boundary conditions – see the paper by Horgan and Chan (1999).

Graded Finite Element Formulation

Displacements for an isoparametric finite element can be written as

$$\mathbf{u}^e = \sum_{i=1}^m N_i \mathbf{u}_i^e \tag{18}$$

where N_i are shape functions, \mathbf{u}_i^e is the nodal displacements corresponding to node i of element e , and m is the number of nodes in an element. For example, for a Q4 element, the standard shape functions are

$$N_i = (1 + \xi \xi_i)(1 + \eta \eta_i)/4, \quad i=1, \dots, 4 \tag{19}$$

where (ξ, η) denote intrinsic coordinates in the interval $[-1, 1]$ and (ξ_i, η_i) denote the local coordinates of node i . Strains are obtained by differentiating displacements as

$$\boldsymbol{\varepsilon}^e = \mathbf{B}^e \mathbf{u}^e, \tag{20}$$

where \mathbf{B}^e is the strain-displacement matrix of shape function derivatives. The strain-stress relations are given by

$$\boldsymbol{\sigma}^e = \mathbf{D}^e(\mathbf{x}) \boldsymbol{\varepsilon}^e, \tag{21}$$

where $\mathbf{D}^e(\mathbf{x})$ is the constitutive matrix, which is a function of spatial position, i.e.

$$\mathbf{D}^e(\mathbf{x}) = \mathbf{D}^e(x, y). \tag{22}$$

The principle of virtual work yields the following finite element stiffness equations (Hughes, 1987):

$$\mathbf{k}^e \mathbf{u}^e = \mathbf{f}^e, \quad \mathbf{k}^e = \int_{\Omega_e} \mathbf{B}^{eT} \mathbf{D}^e(\mathbf{x}) \mathbf{B}^e d\Omega_e \tag{23}$$

where \mathbf{f}^e is the load vector, \mathbf{k}^e is the element stiffness matrix, and Ω_e is the domain of element (e). For the graded element, the $\mathbf{D}^e(\mathbf{x})$ matrix varies spatially within the element. The polynomial order of the matrix will influence the number of Gauss integration points required for the reduced and full integrations. This behavior is investigated in the numerical examples section using two sets of Gauss integration points. A system of algebraic equations is assembled such that

$$\mathbf{K} \mathbf{u} = \mathbf{F}, \quad \mathbf{K}_{ij} = \sum_{e=1}^n \mathbf{k}_{ij}^e, \quad \mathbf{F}_i = \sum_{e=1}^n \mathbf{f}_i^e, \tag{24}$$

where n is the number of elements. The linear system and the derivatives (e.g. strains and stresses) are recovered using standard procedures (Cook *et al.*, 2002).

Two kinds of FEM formulations are used for graded elements: direct Gaussian integration formulation and generalized isoparametric formulation (GIF). These approaches differ on the location that the material properties are sampled in the element: Gauss sampling points for the direct Gaussian formulation (Fig. 5(a)) and nodal sampling points for the GIF (Fig. 5(b)). In this work, we selectively use both formulations.

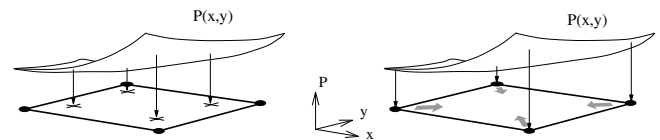


Figure 5. Graded finite elements: (a) Direct Gaussian integration formulation; (b) Generalized isoparametric formulation (Kim and Paulino, 2002a). P denotes a generic property.

Direct Gaussian Integration Formulation

The integral of Eq.(23) is evaluated by Gaussian quadrature, and the matrix $\mathbf{D}^e(\mathbf{x})$ can be directly specified by employing the Young's modulus and the Poisson's ratio at each Gaussian integration point (see Fig. 5(a)). Thus, for 2D problems, the resulting integral becomes

$$\mathbf{k}^e = \sum_i \sum_j \left[\mathbf{B}^{eT} \mathbf{D}^e(\boldsymbol{\xi}) \mathbf{B}^e \right]_{(i,j)} t J W_i W_j, \tag{25}$$

where i and j indicates the corresponding Gauss sampling points in the element, $\boldsymbol{\xi} = (\xi, \eta)$, t denotes thickness, J is the determinant of the Jacobian matrix, i.e. $J = \det(\mathbf{J})$, and W_i is the weight of each Gauss point.

Generalized Isoparametric Formulation (GIF)

The displacements $(u, v) = (u_x, u_y)$ are interpolated for 2-D problems as

$$u = \sum_i N_i u_i, \quad v = \sum_i N_i v_i \tag{26}$$

where the summation is done over the element nodal points. Similarly, the spatial coordinates (x, y) are interpolated as

$$x = \sum_i \hat{N}_i^x x_i, \quad y = \sum_i \hat{N}_i^y y_i \tag{27}$$

Material properties can also be interpolated from the element nodal values by means of shape functions, as illustrated by Fig. 5(b). For instance, the Young's modulus $E = E(\mathbf{x})$ and Poisson's ratio $\nu = \nu(\mathbf{x})$ are given by

$$E = \sum_i \bar{N}_i E_i, \quad \nu = \sum_i \hat{N}_i \nu_i \tag{28}$$

respectively, where \bar{N}_i and \hat{N}_i are appropriate shape functions, which may be distinct from each other. The generalized isoparametric formulation (GIF) concept leads to

$$N = \hat{N} \hat{\epsilon} = \bar{N} = \hat{N}. \tag{29}$$

In this approach, material properties at Gaussian integration points are interpolated from the nodal material properties of the element using isoparametric shape functions, which are the same shape functions as spatial coordinates and displacements.

Numerical Examples

In order to assess convergence and convergence rates of graded finite elements by means of the weak patch test, a set of problems in plane and axisymmetric states are investigated under mesh refinement using both an in-house MATLAB code and the commercial software ABAQUS.

Plane Problems

A few problems in plane stress state are considered where Young's modulus is a function of x , i.e. $E = E(x)$, while the Poisson's ratio is constant. The modulus is assumed to vary exponentially, i.e.

$$E(x) = E_1 e^{\beta x} \tag{30}$$

where $E_1 = E(0)$ and $1/\beta$ is the length scale of the nonhomogeneity characterized by Eq.(2). The applied loading involves fixed-grip, tension, and bending cases. The GIF is used for this study.

Patch Test for Graded Element: Standard or Weak?

Figure 6 shows a 5-element patch of isoparametric, 4-node (Q4), 8-node (Q8) Serendipity (not shown) and 9-node (Q9) Lagrangian (shown) quadrilateral elements under fixed-grip loading. The applied loading corresponds to constant normal strains, i.e. $\sigma_{yy}(x, l) = \epsilon_0 E_1 e^{\beta x}$ where $\epsilon_0 = 1.0$, $E_1 = 1.0$, and $\beta = \log(2)/l$. This stress distribution was obtained by applying nodal forces along the right edge of the finite element mesh. The displacement boundary conditions are prescribed such that $u_y = 0$ in the region $0 \leq x \leq 1$ along $y = 0$ line and, in addition, $u_x = 0$ at either top (for Q4) or middle (for Q8 and Q9) node on the left edge (see Fig. 6).

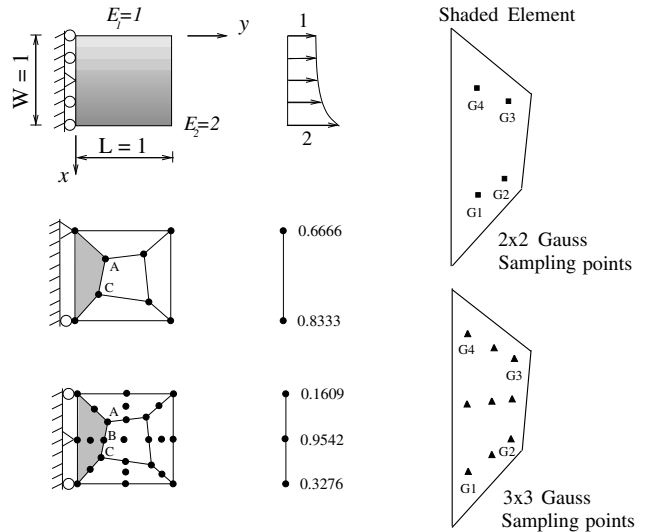


Figure 6. The patch test with 5 graded elements for 4-node, 8-node (not shown) and 9-node (shown) isoparametric quadrilaterals. The applied load corresponds to $\sigma_{yy}(x,1) = \epsilon_0 E_1 e^{\beta x}$ ($\epsilon_0 = 1$, $E_1 = 1.0$, $\beta = \log(2)$) for the fixed grip case. The equivalent nodal loads are shown in the figure.

The following data were used for the finite element analysis:

$$E_1 = 1.0, \nu = 0.3, \tag{31}$$

plane stress, 2 x 2 and 3 x 3 Gauss quadratures

Table 1 compares the FEM results for stresses and displacements with the analytical solutions given by Erdogan and Wu (1997) and in the Section for Exact Solutions (Kim and Paulino, 2002a), respectively. The nodal displacements are calculated at nodes A, B, and C and stresses are computed at the 2 x 2 and 3 x 3 Gaussian integration points as specified in Fig. 6. Table 1 shows that the graded Q4, Q8 and Q9 elements provide slightly inaccurate displacements and stresses with the given level of mesh refinement. One can conclude from the above patch test that the performance of graded elements depends on the degree of mesh refinement corresponding to material gradation and loading conditions. Thus, the patch test needs to be performed for the graded elements by subdividing the mesh. This example justifies the need for the “weak” rather than the “standard” patch test for the graded elements.

Table 1. The patch test with a constant-strain condition using five graded elements (Q4, Q8 and Q9) subjected to fixed-grip loading (see Figure 6). The displacements are $u = u_x$ and $v = u_y$. Generalized isoparametric formulation (GIF) is used for sampling material properties. Exact solutions for the displacements for the Q4 element are different from those for the Q8 and Q9 elements due to different displacement boundary conditions. The numeric precision is $O(10^{-4})$.

Loading Case	Displacements & Stresses	4-node	8-node		9-node	Exact		
		2 x 2	2 x 2	3 x 3	3 x 3	2 x 2(Q4)	2 x 2	3 x 3
Fixed-grip	u_A	-0.0911	0.0602	0.0598	0.0597	-0.0900		0.0600
	v_A	0.3571	0.3516	0.3503	0.3496	0.3500		0.3500
	u_B	-	0.0000	0.0001	0.0001	-		0.0000
	v_B	-	0.2988	0.3007	0.2999	-		0.3000
	u_C	-0.2146	-0.0603	-0.0602	-0.0601	-0.2100		-0.0600
	v_C	0.2540	0.2515	0.2506	0.2501	0.2500		0.2500
	σ_{yy}^{G1}	1.7646	1.6860	1.8216	1.8201		1.6842	1.8164
	σ_{yy}^{G2}	1.6171	1.5731	1.6063	1.6050		1.5714	1.6034
	σ_{yy}^{G3}	1.3183	1.2715	1.2458	1.2451		1.2727	1.2474
	σ_{yy}^{G4}	1.2568	1.1836	1.0988	1.0976		1.1874	1.1011

Weak Patch Test: Q4

Figure 7 shows a non-homogeneous “beam” with exponentially graded modulus subjected to applied load at the right end. The mesh discretization consists of 4×2 , 8×4 , and 16×8 patches of 4-noded isoparametric quadrilateral elements undistorted or distorted according to the geometrical distortion parameter “ d ”. The applied loading corresponds to $\sigma_{yy}(x,10) = \varepsilon_0 E_1 e^{\beta x}$ for fixed grip, $\sigma_{yy}(x,10) =$

1.0 for tension, and $\sigma_{yy}(x,10) = -x+1$ for the bending case, where $\varepsilon_0 = 1.0$, $E_1 = 1.0$, and $\beta = \log(4)/2$. This stress distribution was obtained by applying nodal forces along the right edge of the finite element mesh. The displacement boundary condition is prescribed such that $u_y = 0$ in the region $0 \leq x \leq 2$ along $y = 0$ line and, in addition, $u_x = 0$ for the node in the middle of the left hand side (see Figure 7).

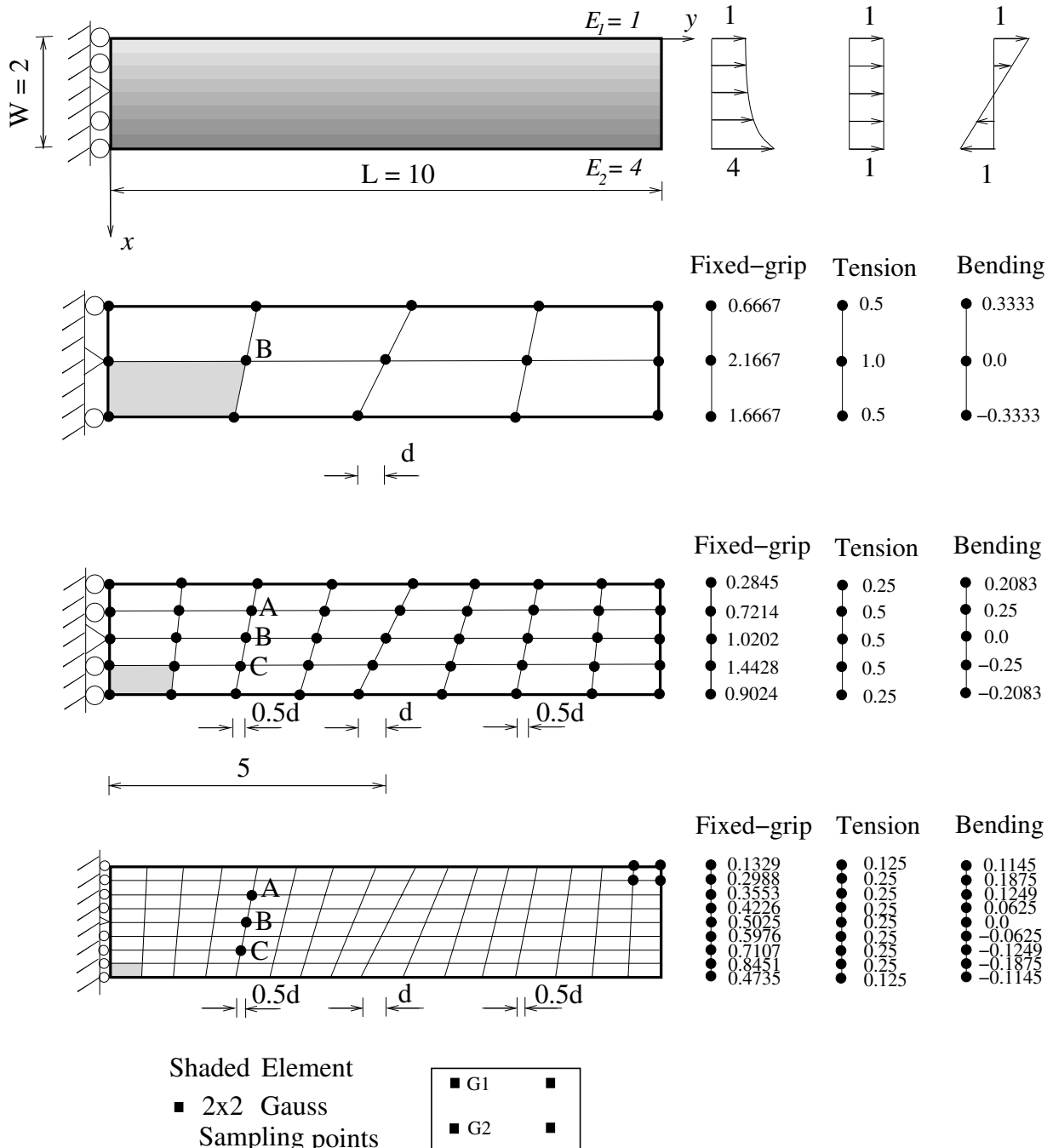


Figure 7. Weak patch test with $M \times N$ elements ($4 \times 2, 8 \times 4, 16 \times 8$) for 4-node isoparametric quadrilaterals (Q4). The meshes are distorted according to the geometric distortion parameter “ d ”. The equivalent nodal loads are shown at the right-hand-side of the corresponding meshes.

The following data are used for the finite element analysis:

$$E_1 = 1.0, \nu = 0.3, \text{ plane stress, } 2 \times 2 \text{ Gauss quadrature} \quad (32)$$

Table 2 compares the FEM results for 4×2 , 8×4 , and 16×8 undistorted ($d = 0$) meshes of the graded Q4 element with the exact solutions. The nodal displacements are calculated at nodes A , B , and C , and stresses are computed at the 2×2 Gaussian integration points as specified in Figure 7. Notice that, for all loading cases, mesh

refinement is needed for acquiring a desired accuracy and it increases the accuracy of FEM results. The accuracy of each individual mesh is better for fixed-grip loading than tension and bending loading cases due to the difference in the nature of boundary conditions. The distorted mesh ($d \neq 0$) gives worse results than undistorted meshes ($d = 0$), and only the case $d = 0$ is investigated in this example. Distorted meshes ($d \neq 0$) are considered in later in this paper.

Table 2. A weak patch test using 4×2 , 8×4 , and 16×8 meshes of undistorted ($d = 0$) Q4 graded elements (see Figure 7). The displacements are $u = u_x$ and $v = u_y$. Generalized isoparametric formulation (GIF) is used for sampling material properties. The numeric precision is $O(10^{-4})$.

Loading Case	Displacement & Stress	4-node			Exact		
		4×2	8×4	16×8	4×2	8×4	16×8
Fixed-grip	uA	-	0.1499	0.1502	0.1500		
	vA	-	2.4999	2.5001	2.5000		
	uB	-0.0003	-0.0001	0.0000	0.0000		
	vB	2.5001	2.4999	2.5000	2.5000		
	uC	-	-0.1501	-0.1500	-0.1500		
	vC	-	2.5000	2.5000	2.5000		
	σ_{yy}^{G1}	2.4227	3.0760	3.4981	2.3154	3.0434	3.4889
	σ_{yy}^{G2}	3.5774	3.7524	3.8655	3.4550	3.7174	3.8562
Tension	uA	-	0.9984	1.1110	1.1585		
	vA	-	1.6649	1.7424	1.7720		
	uB	0.6042	0.8999	1.0189	1.0650		
	vB	1.2184	1.3049	1.3349	1.3460		
	uC	-	0.8331	0.9512	0.9970		
	vC	-	0.9449	0.9273	0.9200		
	σ_{yy}^{G1}	1.0977	1.0830	0.9607	1.0799	1.0103	0.9866
	σ_{yy}^{G2}	1.1820	0.9783	0.8617	0.9315	0.8684	0.9008
Bending	uA	-	1.3696	1.5501	1.6215		
	vA	-	0.7760	0.8779	0.9183		
	uB	0.9062	1.3401	1.5158	1.5854		
	vB	0.1609	0.2399	0.2716	0.2841		
	uC	-	1.3427	1.5180	1.5874		
	vC	-	-0.2960	-0.3347	-0.3500		
	σ_{yy}^{G1}	0.0313	-0.4829	-0.9659	0.0149	-0.5893	-1.0245
	σ_{yy}^{G2}	-0.6119	-1.0996	-1.3688	-0.9898	-1.2642	-1.4149

Weak Patch Test: Q8 and Q9

Figure 8 shows a nonhomogeneous “beam” with exponentially graded modulus subjected to applied load at the right end. The mesh discretization consists of 2×1 , 4×2 , and 8×4 patches of 8-node (Q8) Serendipity (not shown) or 9-node (Q9) Lagrangian (shown) quadrilateral elements. The mesh is distorted according to the geometrical distortion parameter “ d ”.

The applied loading corresponds to $\sigma_{yy}(x,10) = \varepsilon_0 E_I e^{\beta x}$ for fixed grip, $\sigma_{yy}(x,10) = 1.0$ for tension, and $\sigma_{yy}(x,10) = -x+1$ for bending where $\varepsilon_0 = 1.0$, $E_I = 1.0$, and $\beta = \log(4)/2$. This stress distribution was obtained by applying nodal forces along the right edge of the finite element mesh. The displacement boundary condition is prescribed such that $u_y = 0$ in the region $0 \leq x \leq 2$ along $y = 0$ line and, in addition, $u_x = 0$ for the node in the middle of the left hand side (see Figure 8).

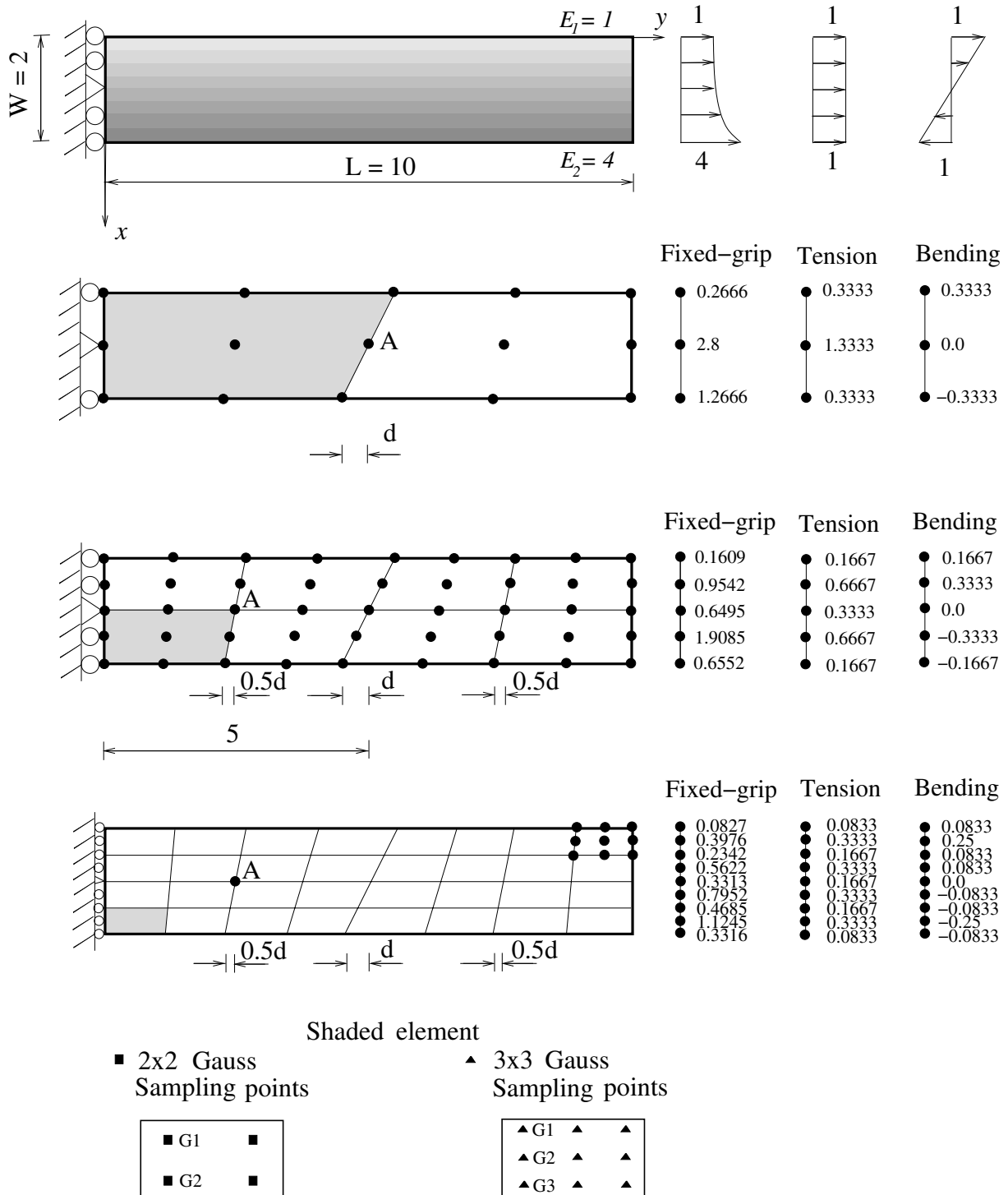


Figure 8. Weak patch test with $M \times N$ elements (2×1 , 4×2 , 8×4) for 8-node (not shown) and 9-node (shown) isoparametric quadrilaterals. The meshes are distorted according to the geometric distortion parameter “ d ”. The equivalent nodal loads are shown at the right-hand-side of the corresponding meshes.

The following data were used for the finite element analysis:

$$E_1 = 1.0, \quad \nu = 0.3, \quad \text{plane stress, } 2 \times 2 \text{ and } 3 \times 3 \text{ Gauss quadratures} \quad (33)$$

Tables 3, 4, and 5 compare the FEM results for the 2×1 , 4×2 , and 8×4 meshes, respectively. The exact solutions include stresses obtained by Erdogan and Wu (1997), and displacements derived by the authors. The nodal displacements are calculated at node A and stresses are computed at the 2×2 and 3×3 Gaussian integration points as specified in Figure 8.

For fixed grip loading case, in general 3 x 3 Gauss quadrature for Q8 and Q9 elements gives better results than 2 x 2 quadrature for Q8 element, and the accuracy increases with mesh refinement. For tension and bending loading cases, 2 x 2 and 3 x 3 Gauss quadratures for Q8 and 3 x 3 Gauss quadrature for Q9 elements give worse results than for those fixed grip loading; however, the accuracy is improved with mesh refinement. Tables 3 to 5 show that both Q8 and Q9 graded elements behave relatively well with

distorted meshes. In general, the effect of the distortion as measured by the parameter d , is reduced with mesh refinement. For the tension case, we observe that a mesh with 16 x 8 elements, although not presented here, leads to the exact results for Q8 elements with both 2 x 2 and 3 x 3 integration rules within $O(10^{-4})$ accuracy. For Q9 elements, the results for the tension case converge for the 8 x 4 mesh (cf. Table 5).

Table 3. A weak patch test with 2 x 1 graded Q8 and Q9 elements (see Figure 8). The displacements are $u = u_x$ and $v = u_y$. Generalized isoparametric formulation (GIF) is used for sampling material properties. The numeric precision is $O(10^{-4})$.

Distortion	Loading Case	Displacements & Stresses	8-node		9-node	Exact	
			2 x 2	3 x 3	3 x 3	2 x 2	3 x 3
d=0	Fixed-grip	u_A	0.0155	-0.0003	-0.0003	0	
		v_A	5.0051	4.9998	4.9998	5	
		σ_{yy}^{G1}	1.3006	1.1380	1.1618	1.3403	1.1691
		σ_{yy}^{G2}	3.0326	1.9999	1.9999	2.9843	2.0
		σ_{yy}^{G3}	-	3.4618	3.4618	-	3.4215
	Tension	u_A	4.7532	4.4318	4.4281	4.2600	
		v_A	2.7463	2.7179	2.7158	2.6920	
		σ_{yy}^{G1}	0.9999	0.9301	0.9300	0.9853	0.9388
		σ_{yy}^{G2}	0.9999	1.0871	1.0863	1.0195	1.0767
		σ_{yy}^{G3}	-	0.9302	0.9300	-	0.9380
	Bending	u_A	6.8655	6.4051	6.3947	6.019	
		v_A	0.6337	0.5940	0.5888	0.5682	
		σ_{yy}^{G1}	0.5773	0.5842	0.5840	0.5449	0.5923
		σ_{yy}^{G2}	-0.5773	0.2376	0.2357	-0.5350	0.2272
		σ_{yy}^{G3}	-	-0.9645	-0.9650	-	-0.9557
d=1	Fixed-grip	u_A	-0.0105	-0.0002	-0.0003	0	
		v_A	4.9935	4.9998	4.9998	5	
		σ_{yy}^{G1}	1.2997	1.1380	1.1380	1.3403	1.1691
		σ_{yy}^{G2}	3.0333	1.9999	1.9999	2.9843	2.0
		σ_{yy}^{G3}	-	3.4618	3.4618	-	3.4215
	Tension	u_A	4.7532	4.4074	4.4466	4.2600	
		v_A	2.7463	2.7144	2.7170	2.6920	
		σ_{yy}^{G1}	0.9999	0.9376	0.9471	0.9853	0.9388
		σ_{yy}^{G2}	0.9999	1.0898	1.0890	1.0195	1.0767
		σ_{yy}^{G3}	-	0.9195	0.9227	-	0.9380
	Bending	u_A	6.8655	6.3496	6.4261	6.019	
		v_A	0.6337	0.5870	0.5898	0.5682	
		σ_{yy}^{G1}	0.5773	0.5940	0.6099	0.5449	0.5923
		σ_{yy}^{G2}	-0.5773	0.2413	0.2404	-0.5350	0.2272
		σ_{yy}^{G3}	-	-0.9779	-0.9758	-	-0.9557

Table 4. A weak patch test with 4 x 2 graded Q8 and Q9 elements (see Figure 8). The displacements are $u = u_x$ and $v = u_y$. Generalized isoparametric formulation (GiF) is used for sampling material properties. The numeric precision is $O(10^{-4})$.

Distortion	Loading Case	Displacements & Stresses	8-node		9-node	Exact	
			2 x 2	3 x 3	3 x 3	2 x 2	3 x 3
d=0	Fixed-grip	uA	0.0053	0.0051	0.0051	0.0	
		vA	2.5065	2.5066	2.5066	2.5	
		σ_{yy}^{G1}	2.3135	2.1620	2.1620	2.3154	2.1625
		σ_{yy}^{G2}	3.4676	2.8335	2.8335	3.4549	2.8284
		σ_{yy}^{G3}	-	3.7103	3.7103	-	3.6993
	Tension	uA	1.0723	1.0676	1.0676	1.0653	
		vA	1.3478	1.3468	1.3468	1.3461	
		σ_{yy}^{G1}	1.0769	1.0789	1.0789	1.0799	1.0812
		σ_{yy}^{G2}	0.9297	1.0407	1.0406	0.9315	1.0408
		σ_{yy}^{G3}	-	0.8731	0.8731	-	0.8730
	Bending	uA	1.5927	1.5857	1.5857	1.5854	
		vA	0.2863	0.2846	0.2846	0.2841	
		σ_{yy}^{G1}	0.0151	0.1221	0.1222	0.0149	0.1221
		σ_{yy}^{G2}	-0.9957	-0.3954	-0.3955	-0.9898	-0.3960
		σ_{yy}^{G3}	-	-1.2465	-1.2465	-	-1.2449
d=1	Fixed-grip	uA	-0.0051	-0.0051	-0.0051	0.0	
		vA	2.5065	2.5066	2.5066	2.5	
		σ_{yy}^{G1}	2.3136	2.1621	2.1621	2.3154	2.1625
		σ_{yy}^{G2}	3.4676	2.8335	2.8335	3.4549	2.8284
		σ_{yy}^{G3}	-	3.7103	3.7103	-	3.6993
	Tension	uA	1.0722	1.0676	1.0676	1.0653	
		vA	1.3476	1.3468	1.3468	1.3461	
		σ_{yy}^{G1}	1.0768	1.0806	1.0789	1.0799	1.0812
		σ_{yy}^{G2}	0.9297	1.0408	1.0406	0.9315	1.0408
		σ_{yy}^{G3}	-	0.8710	0.8731	-	0.8730
	Bending	uA	1.5923	1.5856	1.5857	1.5854	
		vA	0.2855	0.2846	0.2846	0.2841	
		σ_{yy}^{G1}	0.0151	0.1248	0.1222	0.0149	0.1221
		σ_{yy}^{G2}	-0.9957	-0.3952	-0.3955	-0.9898	-0.3960
		σ_{yy}^{G3}	-	-1.2497	-1.2465	-	-1.2449

Table 5. A weak patch test with 8 x 4 graded Q8 and Q9 elements (see Figure 8). The displacements are $u = u_x$ and $v = u_y$. Generalized isoparametric formulation (GIF) is used for sampling material properties. The numeric precision is $O(10^{-4})$.

Distortion	Loading Case	Displacements & Stresses	8-node		9-node	Exact	
			2 x 2	3 x 3	3 x 3	2 x 2	3 x 3
d=0	Fixed-grip	u_A	-0.0002	0.0	0.0	0.0	
		v_A	2.4999	2.5	2.5	2.5	
		σ_{yy}^{G1}	3.0434	2.9411	2.9411	3.0434	2.9411
		σ_{yy}^{G2}	3.7176	3.3635	3.3635	3.7174	3.3635
		σ_{yy}^{G3}	-	3.8467	3.8467	-	3.8467
	Tension	u_A	1.0655	1.0655	1.0655	1.0653	
		v_A	1.3462	1.3461	1.3461	1.3461	
		σ_{yy}^{G1}	1.0102	1.0258	1.0258	1.0103	1.0258
		σ_{yy}^{G2}	0.8681	0.9511	0.9511	0.8684	0.9511
		σ_{yy}^{G3}	-	0.8338	0.8338	-	0.8338
	Bending	u_A	1.5859	1.5855	1.5855	1.5854	
		v_A	0.2841	0.2841	0.2841	0.2841	
		σ_{yy}^{G1}	-0.5895	-0.4960	-0.4960	-0.5893	-0.4960
		σ_{yy}^{G2}	-1.2647	-0.8977	-0.8977	-1.2643	-0.8976
		σ_{yy}^{G3}	-	-1.4046	-1.4046	-	-1.4043
d=1	Fixed-grip	u_A	-0.0002	0.0	0.0	0.0	
		v_A	2.4999	2.5	2.5	2.5	
		σ_{yy}^{G1}	3.0434	2.9411	2.9411	3.0434	2.9411
		σ_{yy}^{G2}	3.7176	3.3635	3.3635	3.7174	3.3635
		σ_{yy}^{G3}	-	3.8467	3.8467	-	3.8467
	Tension	u_A	1.0655	1.0655	1.0655	1.0653	
		v_A	1.3461	1.3461	1.3461	1.3461	
		σ_{yy}^{G1}	1.0102	1.0261	1.0258	1.0103	1.0258
		σ_{yy}^{G2}	0.8681	0.9511	0.9511	0.8684	0.9511
		σ_{yy}^{G3}	-	0.8335	0.8338	-	0.8338
	Bending	u_A	1.5859	1.5855	1.5855	1.5854	
		v_A	0.2841	0.2841	0.2841	0.2841	
		σ_{yy}^{G1}	-0.5896	-0.4956	-0.4960	-0.5893	-0.4960
		σ_{yy}^{G2}	-1.2648	-0.8977	-0.8977	-1.2643	-0.8976
		σ_{yy}^{G3}	-	-1.4051	-1.4046	-	-1.4043

“Higher-Order” Weak Patch Test

Figure 9 compares the ratio of numerical ($v = u_y$) and analytical ($v_{(exact)}$) displacements versus Poisson's ratio (ν) for the bending loading case (see Fig. 2(d)). Both regular ($d = 0$) and distorted ($d = 1$) meshes discretized with Q4, Q8 and Q9 elements are considered using a patch of 4 x 2 elements. The nodal

displacements are evaluated at location *B* in Fig. 7, or location *A* in Fig. 8. Figure 9 shows that both Q8 and Q9 elements converge to the exact solutions independent of the Poisson's ratio, rule of Gauss quadrature, and distortion, while the regular and distorted Q4 elements give significantly inaccurate results. The behavior of Q4 elements can be improved with an incompatible element such as the Q6 and the reader is referred to references (Wilson *et al.*, 1973; Taylor *et al.*, 1976; Cook *et al.*, 2002).

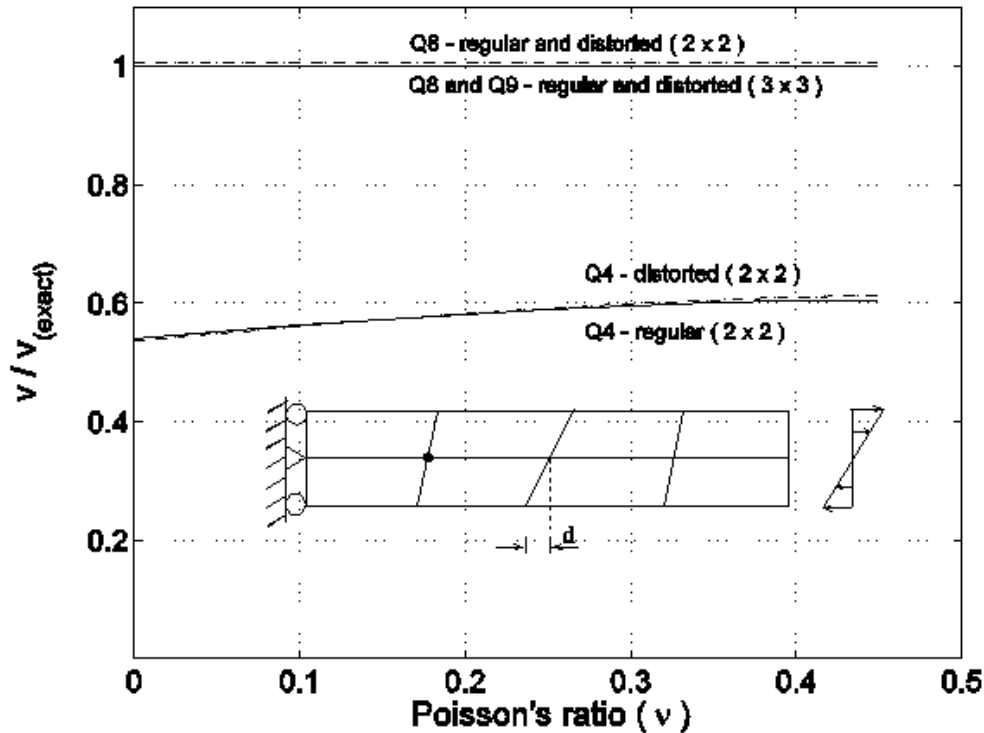


Figure 9. Mesh with 4×2 elements for Q4, Q8, and Q9 elements. The bullet in the insert denotes the point where the displacements are calculated; regular mesh ($d = 0$) and distorted mesh ($d = 1$).

Axisymmetric Problems

Consider the axisymmetric problem of a hollow circular cylinder or disk with the inner radius ($a = 1$) and the outer radius ($b = 2$) subjected to uniform pressure on the inner surface. Patches of 4×4 and 8×8 isoparametric elements are considered here. Figure 10 shows 4-node (Q4) quadrilateral elements and Figure 11 illustrates 8-node (Q8) Serendipity or 9-node (Q9) Lagrangian elements for different distortion factors d ($d = 0$ or $d = 0.1$). The applied loading corresponds to $\sigma_{rr}(1,z) = 1.0$ along $0 \leq z \leq 1$ where “z” denotes the vertical axis from which the inner (a) and outer (b) radii are defined in Figures 10 and 11 (see also Figure 4). This stress distribution was obtained by applying nodal forces along the left edge of the finite element mesh. The displacement boundary condition is prescribed such that $u_z = 0$ for the nodes on the top and bottom edges (see Figs. 10 and 11).

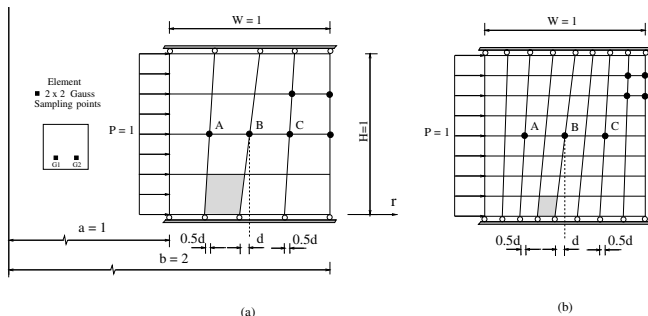


Figure 10. A weak patch test with 4×4 and 8×8 elements for 4-node isoparametric quadrilaterals for axisymmetric problem.

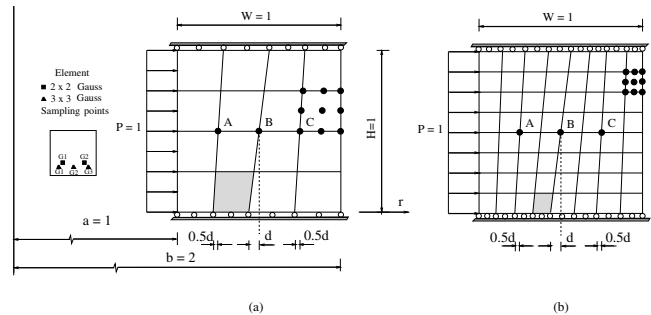


Figure 11. A weak patch test with 4×4 and 8×8 elements for 8-node (not shown) and 9-node (shown) isoparametric quadrilaterals for axisymmetric problem.

Young’s modulus is an exponential function of r as given by Eq. (16), in which n is the nonhomogeneity parameter. The Poisson’s ratio is assumed constant. The direct Gaussian formulation is used for these axisymmetric problems. The following data are used for the FEM analyses:

$$E_1 = 1.0, n = 2, \nu = 0.0, 0.3, \text{ plane stress, } 2 \times 2 \text{ and } 3 \times 3 \text{ Gauss quadratures} \tag{34}$$

Tables 6, 7 ($\nu = 0$) and 8 ($\nu \neq 0$) compare the FEM results with the exact solutions provided by Horgan and Chan (1999). The nodal displacements are calculated at nodes A, B, and C, and stresses are computed at the 2×2 or 3×3 Gaussian integration points as specified in Figs. 10 and 11.

Table 6. A weak patch test with 4 x 4 quadrilateral elements for axisymmetric case ($u = u_r, v = 0$) - see Figures 10 and 11. Direct Gaussian integration method is used for sampling material properties. The numeric precision is $O(10^{-4})$.

Distortion	Displacements & Stresses	4-node	8-node		9-node	Exact	
		2 x 2	2 x 2	3 x 3	3 x 3	2 x 2	3 x 3
d=0	u_A	0.7091	0.7152	0.7152	0.7152	0.7152	
	u_B	0.6457	0.6491	0.6491	0.6491	0.6491	
	u_C	0.6213	0.6237	0.6237	0.6237	0.6237	
	σ_{rr}^{G1}	-0.4307	-0.5624	-0.5778	-0.5778	-0.5625	-0.5907
	$\sigma_{\theta\theta}^{G1}$	0.9064	0.9066	0.9009	0.9009	0.9071	0.9004
	σ_{rr}^{G2}	-0.5314	-0.4137	-0.4999	-0.4999	-0.4137	-0.4848
	$\sigma_{\theta\theta}^{G2}$	0.9538	0.9530	0.9280	0.9280	0.9526	0.9279
	σ_{rr}^{G3}	-	-	-0.3795	-0.3795	-	-0.3908
	$\sigma_{\theta\theta}^{G3}$	-	-	0.9621	0.9621	-	0.9624
d=0.1	u_A	0.7091	0.7083	0.7080	0.7160	0.7152	
	u_B	0.6457	0.6471	0.6470	0.6497	0.6491	
	u_C	0.6213	0.6239	0.6239	0.6244	0.6237	
	σ_{rr}^{G1}	-0.5010	-0.6327	-0.6528	-0.6450	-0.6258	-0.6542
	$\sigma_{\theta\theta}^{G1}$	0.8913	0.8046	0.7966	0.8889	0.8936	0.8890
	σ_{rr}^{G2}	-0.6006	-0.4942	-0.5787	-0.5744	-0.4928	-0.5608
	$\sigma_{\theta\theta}^{G2}$	0.9239	0.8266	0.8080	0.9065	0.9254	0.9070
	σ_{rr}^{G3}	-	-	-0.4701	-0.4706	-	-0.4767
	$\sigma_{\theta\theta}^{G3}$	-	-	0.8248	0.9294	-	0.9304

Table 7. A weak patch test with 8 x 8 quadrilateral elements for axisymmetric case ($u = u_r, v = 0$) - see Figures 10 and 11. Direct Gaussian integration method is used for sampling material properties. The numeric precision is $O(10^{-4})$.

Distortion	Displacements & Stresses	4-node	8-node		9-node	Exact	
		2 x 2	2 x 2	3 x 3	3 x 3	2 x 2	3 x 3
d=0	u_A	0.7136	0.7152	0.7152	0.7152	0.7152	
	u_B	0.6482	0.6491	0.6491	0.6491	0.6491	
	u_C	0.6230	0.6237	0.6237	0.6236	0.6237	
	σ_{rr}^{G1}	-0.4009	-0.4581	-0.4677	-0.4677	-0.4581	-0.4704
	$\sigma_{\theta\theta}^{G1}$	0.9366	0.9366	0.9325	0.9325	0.9366	0.9325
	σ_{rr}^{G2}	-0.4432	-0.3891	-0.4261	-0.4261	-0.3891	-0.4229
	$\sigma_{\theta\theta}^{G2}$	0.9631	0.9630	0.9494	0.9494	0.9630	0.9494
	σ_{rr}^{G3}	-	-	-0.3754	-0.3754	-	-0.3779
	$\sigma_{\theta\theta}^{G3}$	-	-	0.9679	0.9679	-	0.9679
d=0.1	u_A	0.7136	0.7152	0.7152	0.7152	0.7152	
	u_B	0.6482	0.6490	0.6490	0.6490	0.6491	
	u_C	0.6230	0.6236	0.6236	0.6236	0.6237	
	σ_{rr}^{G1}	-0.4829	-0.5374	-0.5483	-0.5482	-0.5374	-0.5504
	$\sigma_{\theta\theta}^{G1}$	0.9121	0.9129	0.9096	0.9096	0.9129	0.9096
	σ_{rr}^{G2}	-0.5265	-0.4757	-0.5108	-0.5108	-0.4757	-0.5082
	$\sigma_{\theta\theta}^{G2}$	0.9301	0.9307	0.9208	0.9208	0.9307	0.9208
	σ_{rr}^{G3}	-	-	-0.4661	-0.4662	-	-0.4679
	$\sigma_{\theta\theta}^{G3}$	-	-	0.9333	0.9333	-	0.9333

Table 8. A weak patch test with 8 x 8 quadrilateral elements for axisymmetric case ($u = u_r, \nu = 0.3$)- see Figures 10 and 11. Direct Gaussian integration method is used for sampling material properties. The numeric precision is $O(10^{-6})$.

Distortion	Displacements & Stresses	4-node	8-node		9-node	Exact	
		2 x 2	2 x 2	3 x 3	3 x 3	2 x 2	3 x 3
d=0.0	u_A	0.8378	0.8403	0.8403	0.8403	0.8403	
	u_B	0.7338	0.7354	0.7354	0.7354	0.7354	
	u_C	0.6775	0.6788	0.6787	0.6788	0.6788	
	σ_{rr}^{G1}	-0.3991	-0.4734	-0.4827	-0.4812	-0.4734	-0.4859
	$\sigma_{\theta\theta}^{G1}$	0.9569	0.9356	0.9300	0.9316	0.9356	0.9289
	σ_{rr}^{G2}	-0.4727	-0.4034	-0.4417	-0.4398	-0.4034	-0.4378
	$\sigma_{\theta\theta}^{G2}$	0.9531	0.9746	0.9537	0.9556	0.9746	0.9549
	σ_{rr}^{G3}	-	-	-0.3890	-0.3867	-	-0.3920
$\sigma_{\theta\theta}^{G3}$	-	-	0.9823	0.9844	-	0.9814	
d=0.1	u_A	0.8380	0.8403	0.8403	0.8402	0.8403	
	u_B	0.7350	0.7354	0.7354	0.7353	0.7354	
	u_C	0.6789	0.6788	0.6787	0.6786	0.6788	
	σ_{rr}^{G1}	-0.4797	-0.5521	-0.5619	-0.5637	-0.5531	-0.5662
	$\sigma_{\theta\theta}^{G1}$	0.9176	0.8967	0.8914	0.8906	0.8959	0.8898
	σ_{rr}^{G2}	-0.5524	-0.4890	-0.5244	-0.5271	-0.4912	-0.5239
	$\sigma_{\theta\theta}^{G2}$	0.9066	0.9286	0.9111	0.9088	0.9262	0.9098
	σ_{rr}^{G3}	-	-	-0.4777	-0.4813	-	-0.4835
$\sigma_{\theta\theta}^{G3}$	-	-	0.9345	0.9308	-	0.9302	

A comparison of the results of Tables 6 and 7 indicate that the 4 x 4 discretization of Figs. 10(a) and 11(a) are too coarse to achieve an accurate solution for this problem. For $\nu = 0.0$ and 8 x 8 mesh (Table 7 and Fig. 10(b)), the 2 x 2 Gauss quadrature for the Q8 gives exact results for all stresses regardless of distortion. Also, the 3 x 3 Gauss quadrature of the Q8 and Q9 elements produces exact results for hoop stresses regardless of distortion, but leads to slightly incorrect results for the radial stress σ_{rr} (see Table 7 and Figs. 10(b) and 11(b)). For $\nu = 0.3$ and 8 x 8 mesh (Table 8 and Figs. 10(b) and 11(b)), the 2 x 2 Gauss quadrature of the Q8 gives exact results for all stresses only for the $d = 0$ case. The 3 x 3 Gauss quadrature of the Q8 and Q9 elements produces slightly incorrect results for all stresses. The behavior of the 2 x 2 and 3 x 3 Gauss quadratures on the radial stresses is consistent with the previous observation about the stress for the tension loading applied parallel to the material gradation (Kim and Paulino, 2002a).

Convergence Rates

This example investigates convergence rates of Q4 and Q8 elements considering an FGM strip under far-field tension loads. Figure 12(a) shows geometry and boundary conditions for a strip with infinite length under far-field tension, and Figure 12(b) shows a plate with finite length under tractions equivalent to the far-field tension (see Eqs.(7) and (10)).

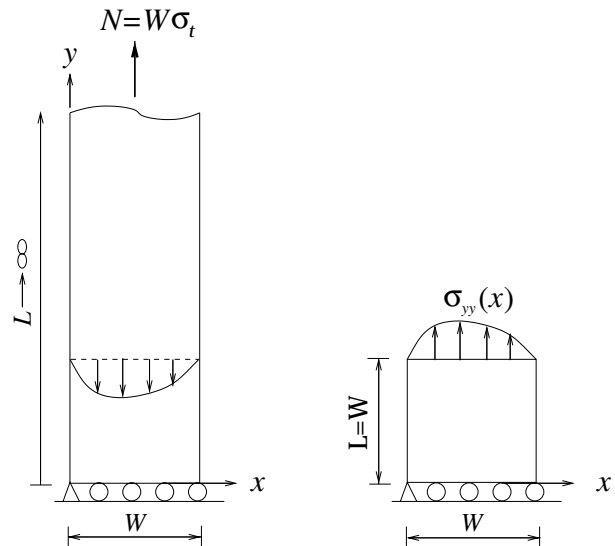


Figure 12. Problem definition: (a) plate with infinite length under far-field constant tension; (b) plate with finite length under exact distribution of tractions that are equivalent to the far-field tension applied to the graded strip ($L/W = 1$).

The applied load is prescribed on the upper edge with normal stress: $\sigma_{yy}(x)$ given by Eq.(7) with appropriate constants A and B . The displacement boundary condition is specified such that $u_y = 0$ along the lower edge, and $u_x = 0$ for the node at the left-bottom corner. Young's modulus is an exponential function of x as given by Eq.(30). The Poisson's ratio is assumed constant. The following data are used for the FEM analyses:

$$\begin{aligned}
 W &= 1, L = 1, \\
 E_1 &= 1.0, E_2 = (3, 5, 7, 10), \nu = 0.3, \\
 \text{plane stress, } 2 \times 2 \text{ and } 3 \times 3 \text{ Gauss quadratures}
 \end{aligned}
 \tag{35}$$

The discretization error can be quantified by the error in the energy norm $\|e\|$ defined as

$$\|e\| = \left(\int_{\Omega} (\boldsymbol{\varepsilon} - \boldsymbol{\varepsilon}_{FE})^T \mathbf{D}(\mathbf{x})(\boldsymbol{\varepsilon} - \boldsymbol{\varepsilon}_{FE}) d\Omega \right)^{1/2}, \tag{36}$$

where $\boldsymbol{\varepsilon}$ and $\boldsymbol{\varepsilon}_{FE}$ are the exact and finite element strain fields, $\mathbf{D}(\mathbf{x})$ is the constitutive matrix of FGMs, and Ω is the domain of the problem.

We use mesh subdivision for assessing convergence rates of Q4 and Q8 elements with the following element discretization along the width (W) and length (L), i.e. 10×10 , 20×20 , and 40×40 elements. The GIF is used for this study. Figure 13 shows the error in the energy norm $\|e\|$ calculated by considering the whole plate for $E_2/E_1 = 3, 5, 7$ and 10 , and also gives useful information on the convergence rate. The notation h denotes the size of the square element used. The 8-node (Q8) quadrilateral elements with 3×3 and 2×2 Gauss quadrature provide higher accuracy and convergence rates than those for 4-node (Q4) quadrilateral elements.

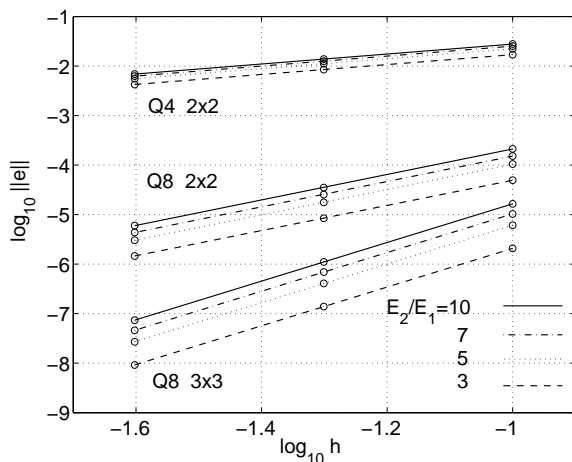


Figure 13. Error in the energy norm $\|e\|$ of the problem for $E_2/E_1 = 3, 5, 7$, and 10 . The energy norm is calculated considering all the elements ($L/W = 1.0$).

Stability Considerations

Two kinds of investigations are made regarding the stability analysis. First, basic deformation modes (tension, bending, and shear) are studied, and then, an eigenanalysis is performed at the element level (eigenvalue test). The latter test can detect zero-energy deformation modes, lack of invariance (with respect to geometrical orientation), and absence of rigid body motion capability; and can also provide an estimation of the relative quality of competing elements. In these investigations, the graded element is compared with the homogeneous element. The direct Gaussian formulation is used for this study.

Single Element Test - Basic Deformation Modes

The strain energy stored in the Q4 and Q8 elements is compared for homogeneous and graded elements considering tension, pure shear, and pure bending deformation modes. For the sake of

reference, Figure 14 shows imposed displacements for different deformation modes for homogeneous materials ($\beta = 0$), while Figs. 15 and 16 illustrate the deformations for $\beta = 1.0, 0.5, -1.0$. In order to represent tension, shear, and pure bending deformation in FGMs ($\beta \neq 0$), the exact solutions to displacements are proportionally factored to give $\Delta = 0.1$ as the single displacement at the node indicated in Figures 14 to 16. Note that deformation-equivalent loads are different for homogeneous and FGM cases.

Figure 14 represents well-known and expected results for homogeneous materials ($\beta = 0$). In Figs. 14 and 16, notice that the material gradation β has a significant influence on the deformation mode. Figure 15 shows that for the tension case, if $\Delta = 0.1$ is imposed at the left-top corner node, then the deformed shape scales with β (cf. the first two cells of the first row) and is significantly changed if β changes sign, i.e. reversal of gradation (cf. compare the first two cells with the third cell). If $\Delta = 0.1$ is imposed at the right-top corner, the deformed shapes are consistent with those just described above, i.e. the first and second rows of cells of Figure 15. Notice that if $\beta > 0$ the reference displacement (Δ) is in the weak material side, while if $\beta < 0$ it is on the strong material side. A comparison between the first cell of the first row of Figure 14(a) ($\beta = 0$) and those cells of Figure 15 ($\beta \neq 0$) indicate that the deformed shapes in FGMs can be counter-intuitive as bending-type deformation develops for purely applied tension load.

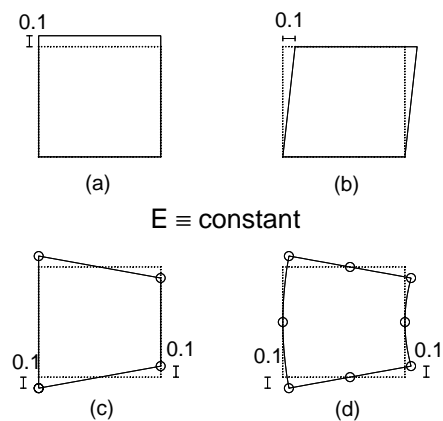


Figure 14. Imposed displacement vectors for homogeneous materials ($\nu = 0$): (a) tension, (b) pure shear, (c) pure bending for Q4, and (d) bending for Q8.

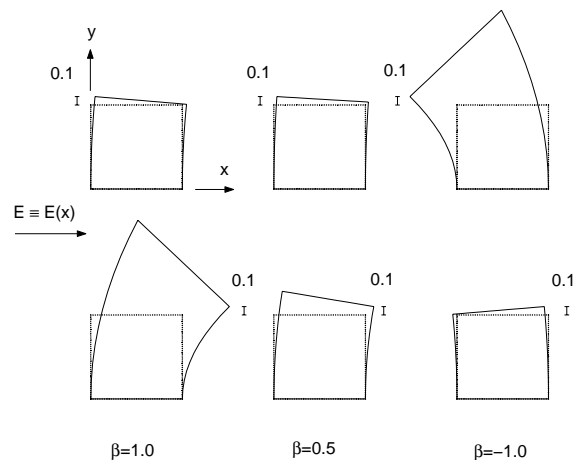


Figure 15. Imposed displacement vectors to give $\Delta = 0.1$ at the node indicated for tension applied perpendicular to the material gradation ($\beta = 1.0, 0.5, -1.0$ and $\nu = 0$).

Figure 16 illustrates various deformation modes for FGMs ($\beta \neq 0$) considering $\nu = 0$. The cells in the first row illustrates deformation modes under tension loading for $E=E(y)$. Differently from the configuration observed in Figure 15, there is no bending deformation in the cells of Figure 16(a), independent of the β value. This difference is due to the orientation of material gradation in each case. Figure 16(b) shows deformed shapes for the pure bending loading considering $E=E(x)$ and $\beta=1.0, 0.5$, and -1.0 . The reference deformation is $\Delta = 0.1$ at the bottom-right corner. It is interesting to observe the shift in the middle point of the bottom-edge (cf. solid and hollow bullets) as a function of the material gradation parameter β . The hollow dot represents a point in the homogeneous material, which does not move upon bending deformation (cf. Fig. 14(d)) and thus indicates the neutral axis location for this configuration. The solid dot represents the FGM case and, differently from the homogeneous case, the point shifts as a function of the material gradation. For example, according to Fig. 16(b)

$$\begin{aligned} \beta > 0, & \quad u_x > 0, \quad u_y < 0. \\ \beta < 0, & \quad u_x > 0, \quad u_y > 0. \end{aligned}$$

Notice that the reference point shifts down for $\beta > 0$ and it shifts up for $\beta < 0$. Figure 16(c) shows deformed shapes for pure shear loading considering $E=E(y)$ and $\beta=1.0, 0.5$, and -1.0 . Notice that the curvature of the edges that were vertical in the original configuration changes when β changes sign.

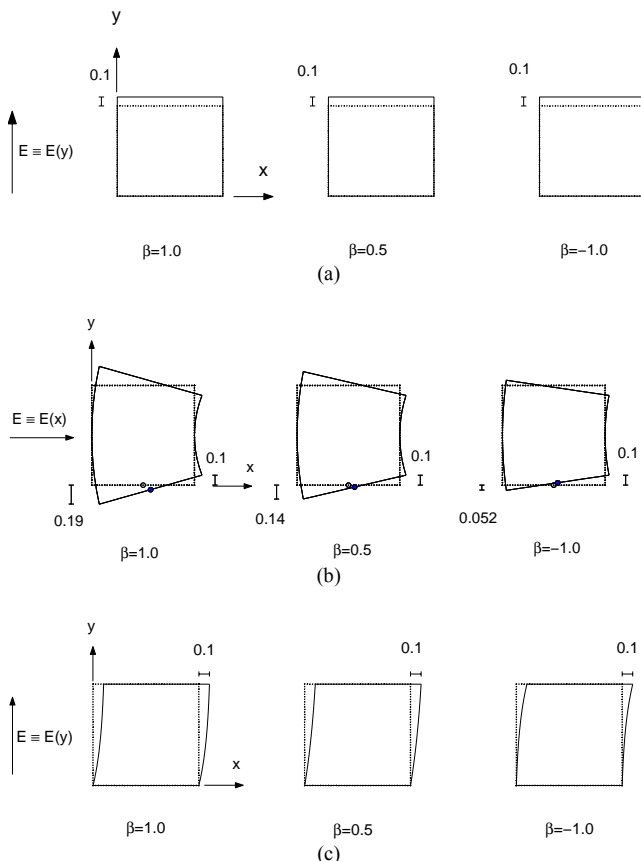


Figure 16. Imposed displacement vectors to give $\Delta = 0.1$ at the point indicated for $\beta = 1.0, 0.5, -1.0$ and material gradation as shown above ($\nu = 0$). (a) tension; (b) bending; (c) shear.

Table 9 summarizes the strain-energy values induced by the above exactly imposed displacements. Imposed displacements for Q4 and Q8 elements are different from the exact imposed displacements because of approximating function characteristics of elements. In other words, nodal displacements for both elements are imposed exactly, but displacements among nodes inside an element are interpolated using shape functions. All the results are normalized with respect to the strain energy for the homogeneous material ($\beta = 0$). This table shows that the order of integration can have a significant impact in the FEM results (cf. 1×1 versus 2×2 for Q4 and 2×2 versus 3×3 for Q8). Thus reduced integration for graded elements should be used with great care. Neglecting the reduced integration for the Q4, we observe that, for the bending case, the strain energy for the FGM ($\beta \neq 0$) is always lower than or equal to that for the homogeneous material ($\beta = 0$). The results are functions of the material gradation parameter β .

Table 9. Strain energy ratio of the FEM results for the FGM with respect to the exact solution for the homogeneous material induced by the imposed displacements (Case(a): displacement $\Delta = 0.1$ imposed at the top-left corner; Case(b): displacement $\Delta = 0.1$ imposed at the top-right corner).

Case	β	4-node		8-node	
		1×1	2×2	2×2	3×3
Tension $E(y)$	0	1.000	1.000	1.000	1.000
	0.5	1.042	1.085	0.999	1.001
	1.0	1.175	1.377	1.003	1.022
	-1.0	1.175	1.376	1.003	1.022
Tension $E(x)$ Case (a)	0	1.000	1.000	1.000	1.000
	0.5	1.041	1.040	0.998	1.000
	1.0	1.153	1.444	0.986	1.000
	-1.0	1.152	1.144	0.986	1.000
Tension $E(x)$ Case (b)	0	1.000	1.000	1.000	1.000
	0.5	1.040	1.040	0.999	1.000
	1.000	1.153	1.144	0.986	1.000
	-1.0	1.154	1.146	0.985	1.000
Shear $E(y)$	0	1.000	1.000	1.000	1.000
	0.5	1.043	1.085	1.000	1.001
	1.0	1.175	1.377	1.003	1.022
	-1.0	1.167	1.372	1.004	1.023
Bending $E(x)$	0	0.000	1.501	1.000	1.000
	0.5	0.833	1.494	0.968	1.000
	1.0	0.303	1.481	0.876	0.997
	-1.0	0.289	1.449	0.877	0.992

Spectral Analysis - Eigenvalue Test

The eigenvalue test is performed for the single element stability check. The test can detect zero energy deformation modes (both rigid body and spurious modes). The element is not constrained so that the element stiffness matrix \mathbf{k}^e is the complete matrix. Thus three independent rigid-body motions exist in the plane, and three of the eigenvalues should be zero for a plane element. In addition, zero-energy or spurious singular modes also yield zero eigenvalues.

The element is square, and its length and width are 1.0 with the origin ($x = y = 0$) at the left-bottom-corner node. In the element, Young's modulus is given by Eq.(30) with $E_1 = 1.0$ (normalized), and $\beta = 0.0$ (homogeneous) and 1.0 (nonhomogeneous material). The Poisson's ratio is assumed to be constant, i.e. $\nu = 0.3$.

Figures 17 to 22 illustrate the results of the spectral analysis for the Q4, Q8, and Q9 considering $\beta=0$ (homogeneous material) and

$\beta=1.0$ (FGM). A comparison between the results for homogeneous materials and FGMs leads to the following observations:

- As expected, the number of rigid-body modes (three) is the same for both homogeneous and graded elements

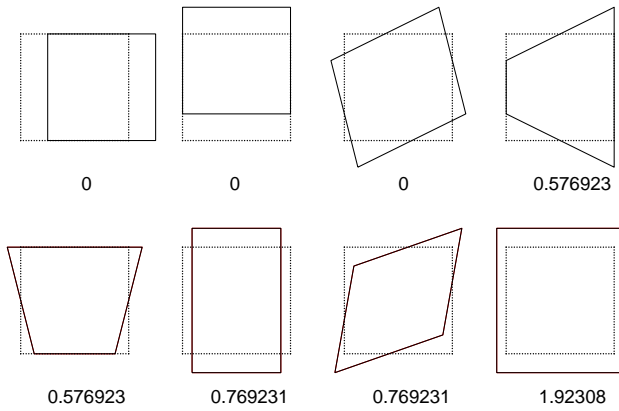


Figure 17. Eigen-analysis for Q4 (2 x 2 Gauss quadrature) with $\beta = 0$ (homogeneous material). The numbers indicate the eigenvalues (λ_i). Compare with Figure 18.

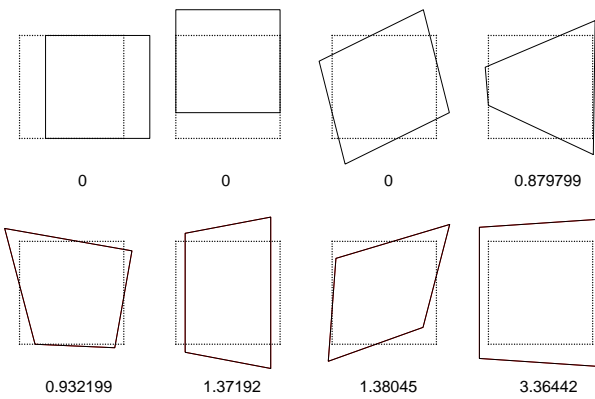


Figure 18. Eigen-analysis for Q4 (2 x 2 Gauss quadrature) with $\beta = 1$ (FGM). The numbers indicate the eigenvalues (λ_i). Compare with Figure 17.

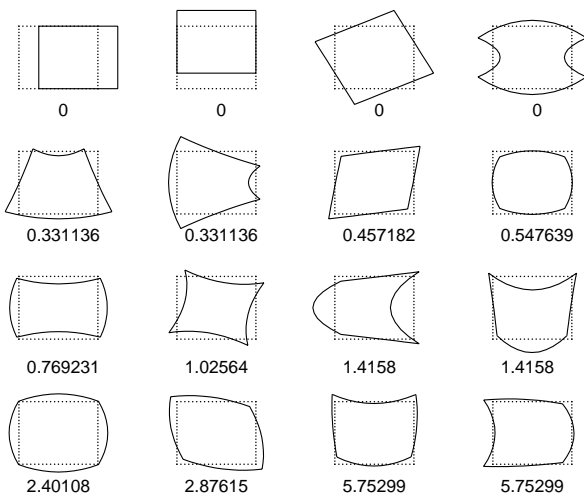


Figure 19. Eigen-analysis for Q8 (2 x 2 Gauss quadrature) with $\beta = 0$ (homogeneous material). The numbers indicate the eigenvalues (λ_i). Compare with Figure 20.

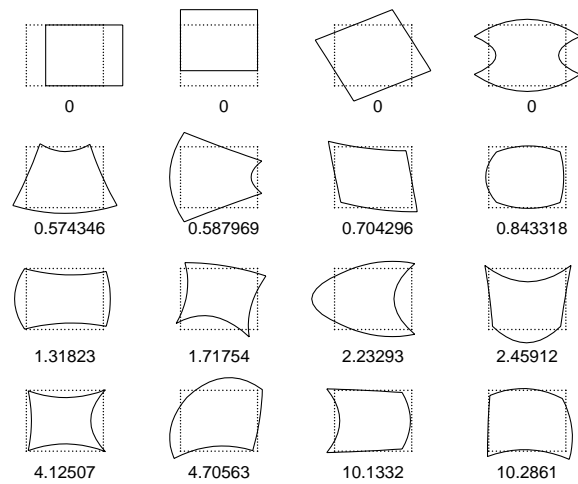


Figure 20. Eigen-analysis for Q8 (2 x 2 Gauss quadrature) with $\beta = 1$ (FGM). The numbers indicate the eigenvalues (λ_i). Compare with Figure 19.

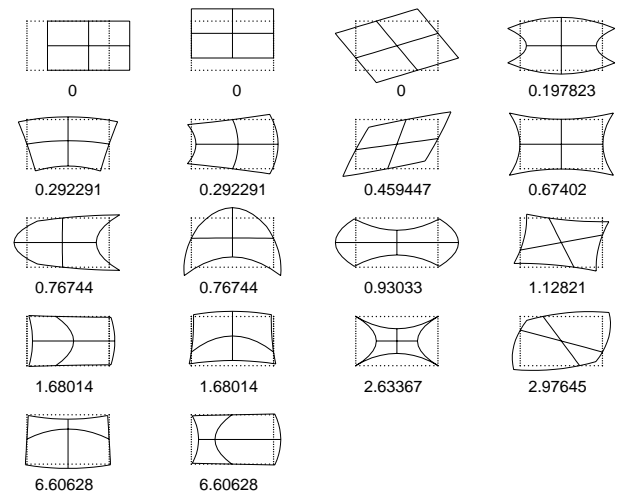


Figure 21. Eigen-analysis for Q9 (3 x 3 Gauss quadrature) with $\beta = 0$ (homogeneous material). The numbers indicate the eigenvalues (λ_i). Compare with Figure 22.

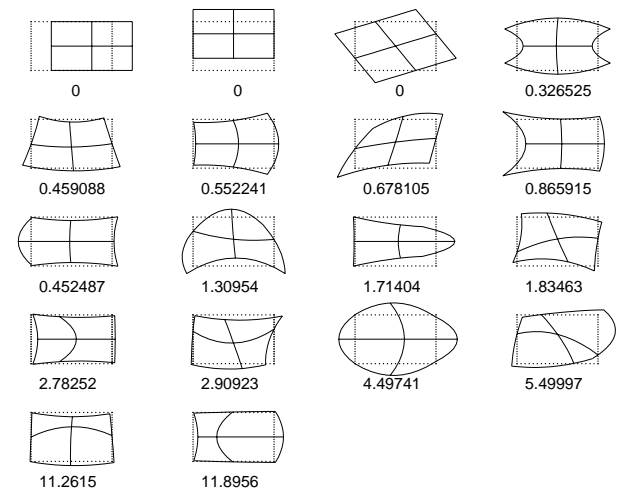


Figure 22. Eigen-analysis for Q9 (3 x 3 Gauss quadrature) with $\beta = 1$ (FGM). The numbers indicate the eigenvalues (λ_i). Compare with Figure 21.

- The number of spurious deformation (zero energy) modes is also the same for both homogeneous and graded elements, i.e. two spurious modes for Q4 with order of quadrature 1, one for Q8 with 2 x 2 Gauss integration, and three for Q9 with 2 x 2 Gauss integration
- Symmetry, as expressed by the deformation modes (eigenvectors), is broken for graded elements, i.e. there are no repeated eigenmodes or repeated eigenvalues as in the homogeneous element.
- The total energy ($U_i = \lambda_i/2$, $i=1, \dots, \text{NDOFs}$) increases for the FGM with $\beta > 0$ in comparison with that for the homogeneous material. Here NDOFs indicates the number of degrees of freedom in the element.

Conclusions

Once an element passes the patch test with a consistency and a stability check, convergence is assured as the size of elements tend to zero. The original patch test considers constant strain or stress state for conventional homogeneous finite elements. However, for nonhomogeneous materials, consistency and stability of graded finite elements are verified in the context of the weak patch test. In the preceding sections, convergence and convergence rates of the Q4, Q8, and Q9 graded elements (for both plane and axisymmetric problems) to the exact solutions have been studied under subdivision of finite elements.

This study indicates that, in general, 3 x 3 Gauss Quadrature for Q8 and Q9 elements shows better performance than 2 x 2 Gauss Quadrature for Q4, and that Q4 elements need to be used with care due to low convergence rates. Moreover, the stability investigation reveals that one should be very careful when using homogeneous elements with piecewise constant material properties to model nonhomogeneous materials. This paper has shown that the deformation modes (and associated strain energy) for graded elements (Figure 1(c)) are quite different from those for homogeneous elements (Figure 1(d)). Thus poor numerical results may be obtained when homogeneous elements are used instead of graded elements, especially when relatively coarse meshes are used to model FGMs.

Acknowledgements

We gratefully acknowledge the support from the National Science Foundation (NSF) under grant No. CMS-0115954 (Mechanics and Materials Program) and from the NASA Ames Research Center (NAG 2-1424) to the University of Illinois at Urbana-Champaign. At NASA, Dr. Tina Panontin serves as the project Technical Monitor. The second author acknowledges the start-up support from University of Connecticut. Any opinions expressed herein are those of the writers and do not necessarily reflect the views of the sponsors.

References

Almajid, A., Taya, M., and Hudnut, S., 2001, "Analysis of out-of-plane displacement and stress field in a piezocomposite plate with functionally graded microstructure," *International Journal of Solids and Structures*, 38(19):3377--3391.

Anlas, G., Santare, M.H., and Lambros, J., 2000 "Numerical calculation of stress intensity factors in functionally graded materials," *International Journal of Fracture*, 104:131--143.

Auricchio, F. and Taylor, R. L., 1993, "Linked interpolation for Reissner-Mindlin plate elements: Part II -- A simple triangle," *International Journal for Numerical Methods in Engineering*, 36:3057--3065.

Auricchio, F. and Taylor, R. L., 1994, "A shear deformable plate element with an exact thin limit," *Computer Methods in Applied Mechanics and Engineering*, 118:393--412.

Babuska, I. and Strouboulis, T., 2001, *The finite element method and its reliability*, Oxford University Press Inc., New York, 2001.

Bathe, K.J., 1995, *Finite element procedures*. Prentice Hall, 1995.

Bazeley, G.P., Cheung, Y.K., Irons, B. M., and Zienkiewicz, O. C., 1966, "Triangular elements in plate bending. Conforming and nonconforming solutions," *Proceedings of the First Conference on Matrix Methods In Structural Mechanics*, AFFDLTR-CC-80, Wright Patterson A. F. Base, Ohio, pp 547--576.

Becker, T. L., Cannon, R. M., and Ritchie, R. O., 2000, "An approximate method for residual stress calculation in functionally graded materials," *Mechanics of Materials*, 32(2):85--97.

Belytschko, T. and Lasry, D., 1988, "A fractal patch test," *International Journal for Numerical Methods in Engineering*, 26:2199--2210.

Belytschko, T., Liu, W.K., and Moran, B., 2000, *Nonlinear finite elements for continua and structures*, John Wiley & Sons.

Carbonari, R.C., Silva, E.C.N., and Paulino, G.H., 2006a, "Design of functionally graded piezoelectric actuators using topology optimization. In: Modeling, Signal Processing, and Control - 13th SPIE (Annual Symposium on Smart Structures and Materials), 2006, San Diego. Proceedings of Modeling, Signal Processing and Control - 13th SPIE.

Carbonari, R.C., Silva, E.C.N., and Paulino, G.H., 2006b, "Multi-actuated functionally graded piezoelectric micro-tools design using topology optimization. In: Modeling, Signal Processing, and Control - 13th SPIE (Annual Symposium on Smart Structures and Materials), 2006, San Diego. Proceedings of Modeling, Signal Processing and Control - 13th SPIE.

Carpenter, R.D., Liang, W.W., Paulino, G.H., Gibeling, J.C., and Munir, Z.A., 1999, "Fracture testing and analysis of a layered functionally graded Ti/TiB beam in 3-point bending," *Materials Science Forum*, 308--311(1):837--842.

Cheung, W.K., Zhang, Y.X., and Chen, W.J., 2002, "A refined nonconforming plane quadrilateral element," *Computers & Structures*, Elsevier: U.K., 78:699--709.

Cho, J.R. and Oden, J.T., 2000, "Functionally graded material: a parametric study on thermal-stress characteristics using Crank-Nicolson-Galerkin scheme," *Computer Methods in Applied Mechanics and Engineering*, 188(1-3):17--38.

Cho, J.R. and Ha, D.Y., 2001, "Thermo-elastoplastic characteristics of heat-resisting functionally graded composite structures," *Structural Engineering and Mechanics*, 11(1):49--70.

Cook, R.D., Malkus, D.S., Plesha, M.E., and Witt, R., 2002, *Concepts and applications of finite element analysis*, 4th Edition. John Wiley & Sons.

Dao, M., Gu, P., Maewal, A., and Asaro, R.J., 1997, "A micromechanical study of residual stresses in functionally graded materials," *Acta Materialia*, 45(8):3265--3276.

Eischen, J.W., 1987, "Fracture of nonhomogeneous materials," *International Journal of Fracture*, 34:3--22.

Erdogan, F. and Wu, B.H., 1997, "The surface crack problem for a plate with functionally graded properties," *ASME Journal of Applied Mechanics*, 64:449--456.

Giannakopoulos, A.E., Suresh, S., Finot, M., and Olsson, M., 1995, "Elastoplastic analysis of thermal cycling: layered materials with compositional gradients," *Acta Materialia*, 43(4):1335--1354.

Grujicic, M. and Zhang, Y., 1998, "Determination of effective elastic properties of functionally graded materials using Voronoi cell finite element method," *Materials Science and Engineering A*, 251(1-2): 64--76.

Gu, P., Dao, M., and Asaro, R.J., 1999, "A simplified method for calculating the crack-tip field of functionally graded materials using the domain integral," *ASME Journal of Applied Mechanics*, 66(1):101--108.

Herrmann, N., 1989, "The patch test for shell elements," *Zeitschrift für Angewandte Mathematik und Mechanik*, East Germany, 69:250--252.

Horgan, C.O. and Chan, A.M., 1999, "The pressurized hollow cylinder or disk problem for functionally graded isotropic linearly elastic materials," *Journal of Elasticity*, 55:43--59.

Hughes, T.J.R., 1987, *The finite element method: linear static and dynamic finite element analysis*, Prentice-Hall, New Jersey.

Irons, B.M., 1966, "Numerical integration applied to finite element methods," *Conference on Use of Digital Computers in Structural Engineering*, University of Newcastle.

Irons, B.M. and Razaque, A., 1972, "Experience with the patch test for convergence of finite element methods," In Aziz, A.K. (ed.), *Mathematical Foundations of the Finite Element Method*, Academic Press, pp 557--587.

Jin, Z.H., Paulino, G.H., and Dodds, Jr. R.H., 2002, "Finite element investigation of quasi-static crack growth in functionally graded materials using a novel cohesive zone fracture model," *ASME Journal of Applied Mechanics*, 69(3):370-379.

- Jitcharoen, J., Padture, N.P., Giannakopoulos, A.E., and Suresh, S., 1998, "Hertzian-crack suppression in ceramics with elastic-modulus-graded surfaces," *Journal of the American Ceramic Society*, 81(9):2301--2308.
- Ju, S.B. and Sin, H.C., 1996, "New incompatible four-noded axisymmetric elements with assumed strains," *Computers & Structures*, Elsevier: U.K., 60:269--278.
- Khor, K.A. and Gu, Y.W., 2000, "Effects of residual stress on the performance of plasma sprayed functionally graded $ZrO_2/NiCoCrAlY$ coatings," *Materials Science and Engineering A*, 277(1-2):64--76.
- Kim, A.S., Suresh, S., and Shih, C.F., 1997, "Plasticity effects on fracture normal to interfaces with homogeneous and graded composites," *International Journal of Solids and Structures*, 34(26):3415--3432.
- Kim, J.-H., Paulino, G.H., 2002a, "Isoparametric graded finite elements for nonhomogeneous isotropic and orthotropic materials," *ASME Journal of Applied Mechanics*, 69(4):502--514.
- Kim J.-H., Paulino G. H., 2002b, "Finite element evaluation of mixed mode stress intensity factors in functionally graded materials," *International Journal for Numerical Methods in Engineering*, 53(8):1903--1935.
- Kim J.-H. and Paulino G. H., 2003, "T-stress, Mixed-mode Stress Intensity Factors, and Crack Initiation Angles in Functionally Graded Materials: A Unified Approach Using the Interaction Integral Method," *Computer Methods in Applied Mechanics and Engineering*, 192 (11-12): 1463-1494.
- Kim J.-H. and Paulino G. H., 2004, "Simulation of Crack Propagation in Functionally Graded Materials under Mixed-mode and Non-proportional Loading," *International Journal of Mechanics and Materials in Design*, 1(1):63-94.
- Kim J.-H. and Paulino G. H., 2005, "Consistent Formulations of the Interaction Integral Method for Fracture of Functionally Graded Materials," *Journal of Applied Mechanics*, 72(3):351-364.
- Leßle, P., Dong, M., and Schmauder, S., 1999, "Self-consistent matrixity model to simulate the mechanical behavior of interpenetrating microstructures," *Computational Materials Science*, 15:455--465.
- Lee, Y.D. and Erdogan, F., 1995, "Residual/thermal stresses in FGM and laminated thermal barrier coatings," *International Journal of Fracture*, 69:145--165.
- Lin, J.S. and Miyamoto, Y., 2000, "Notch effect of surface compression and the toughening of graded $Al_2O_3/TiC/Ni$ materials," *Acta Materialia*, 48(3):767--775.
- Loikkanen, M.J. and Irons, B.M., 1984, "An 8-node brick finite element," *International Journal for Numerical Methods in Engineering*, 20:523--528.
- Martins, R.A.F. and Sabino, J., 1997, "A simple and effective triangular finite element for plate bending," *Engineering Computations*, MCB University Press: U.K., 14:883--900.
- Noda, N., 1999, "Thermal stresses in functionally graded materials," *Journal of Thermal Stresses*, 22(1):477--512.
- Park, Y.M. and Choi, C.K., 1997, "The patch tests and convergence for nonconforming Mindlin plate bending elements," *Structural Engineering & Mechanics*, Techno-Press: South Korea, 5:471--490.
- Paulino G. H. and Kim J.-H., 2004, "A New Approach to Compute T-stress in Functionally Graded Materials Using the Interaction Integral Method," *Engineering Fracture Mechanics*, 71 (13-14):1907-1950.
- Piltner, R. and Taylor, R.L., 2000, "Triangular finite elements with rotational degrees of freedom and enhanced strain modes," *Computers & Structures*, Elsevier: U.K., 75:361--368.
- Pindera, M.J. and Dunn, P., 1997, "Evaluation of the higher-order theory for functionally graded materials via the finite-element method," *Composites Part B, Engineering*, 28(1/2):109--119.
- Razzaque, A., 1986, "The patch test for elements," *International Journal for Numerical Methods in Engineering*, 22:63--71.
- Samuelsson, A., Rydholm, S., and Wiberg, N.E., 1987, "On the practical use of standard and higher order patch tests for plate bending problems," *Proceedings of the First International Conference of Reliability and Robustness of Engineering Software*, Como, Italy, pp 343--351.
- Santare, M.H. and Lambros, J., 2000, "Use of graded finite elements to model the behavior of nonhomogeneous materials," *ASME Journal of Applied Mechanics*, 67:819--822.
- Schmauder, S. and Weber, U., 2001, "Modelling of functionally graded materials by numerical homogenization," *Archive of Applied Mechanics*, 71:182--192.
- Shen, Y.L., 1998, "Thermal expansion of metal-ceramic composites: a three-dimensional analysis," *Materials Science and Engineering A*, 252(2):269--275.
- Stephens, L.S., Liu, Y., and Meletis, E.I., 2000, "Finite element analysis of the initial yielding behavior of a hard coating/substrate system with functionally graded interface under indentation and friction," *Journal of Tribology-Transactions of the ASME*, 122(2):381--387.
- Strang, G., 1972, "Variational crimes and the finite element method," In Aziz, A.K. (ed). *Proceedings of Foundations of the Finite Element Method*, Academic Press, pp 689--710.
- Strang, G. and Fix, G.F., 1973, *An analysis of the finite element method*, Prentice Hall, 1973.
- Tanaka, K., Watanabe, H., Sugano, Y., and Poterasu, V.F., 1996, "A multicriterial material tailoring of a hollow cylinder in functionally graded materials: Scheme to global reduction of thermoelastic stresses," *Computer Methods in Applied Mechanics and Engineering*, 135(3-4):369--380.
- Taylor, R.L., Beresford, P.J., and Wilson, E.L., 1976, "A nonconforming element for stress analysis," *International Journal for Numerical Methods in Engineering*, 10:1211--1219.
- Taylor, R.L., Zienkiewicz, O.C., Simo, J.C., and Chan, A., 1986, "The patch test -- A condition for assessing FEM convergence," *International Journal for Numerical Methods in Engineering*, 22:39--62.
- Timoshenko, S.P. and Goodier, J.N., 1987, *Theory of Elasticity*, 3rd Edition. McGraw-Hill, New York.
- Williamson, R.L., Rabin, B.H., and Drake, J.T., 1993, "Finite element analysis of thermal residual stresses at graded ceramic-metal interfaces. Part I: model description and geometric effects," *ASME Journal of Applied Physics*, 74:1310--1320.
- Wilson, E.L., Taylor, R.L., Doherty, W.P., and Ghaboussi, J., 1973, "Incompatible displacement models," *Numerical and Computer Methods in Structural Mechanics*, Academic Press, New York, pp 43--57.
- Wu, Z. and Chen, D.P., 1997, "The patch test conditions and some multivariable finite element formulations," *International Journal for Numerical Methods in Engineering*, 40:3015--3032.
- Zhang, Z. and Paulino, G.H., 2005, "Cohesive zone modeling of dynamic failure in homogeneous and functionally graded materials," *International Journal of Plasticity*, 21:1195-1254.
- Zhifei, L., 1993, "Generalized conforming triangular elements for plate bending," *Communications in Numerical Methods in Engineering*, 9:53--65.
- Zienkiewicz, O.C. and Lefebvre, D., 1988, "A robust triangular plate bending element of the Reissner-Mindlin type," *International Journal for Numerical Methods in Engineering*, 26:1169--1184.
- Zienkiewicz, O.C. and Taylor, R.L., 1997, "The finite element patch test revisited: A computer test for convergence, validation and error estimates," *Computer Methods in Applied Mechanics and Engineering*, 149:223--254.
- Zienkiewicz, O.C. and Taylor, R.L., 2000, *The finite element method*, 5th Edition. Butterworth-Heinemann, Oxford, Volume 1, Chapter 10.
- Zienkiewicz, O.C., Qu, S., Taylor, R.L., and Nakazawa, S., 1986, "The patch test for mixed formulations," *International Journal for Numerical Methods in Engineering*, 23:1873--1883.
- Zienkiewicz, O.C., Xu, Z., Zeng, L.F., Samuelson, A., and Wiberg, N.E., 1993, "Linked interpolation for Reissner-Mindlin plate elements: Part I -- A simple quadrilateral," *International Journal for Numerical Methods in Engineering*, 36:3040--3056.